Available online at www.sciencedirect.com
ScienceDirect
Geochimica et Cosmochimica Acta 71 (2007) 4342–4364
Geochimica et Cosmochimica Acta
www.elsevier.com/locate/gca

Type C Ca, Al-rich inclusions from Allende: Evidence for multistage formation

Alexander N. Krot [a,*], Hisayoshi Yurimoto [b], Ian D. Hutcheon [c], Guy Libourel [d,e], Marc Chaussidon [d], Laurent Tissandier [d], Michael I. Petaev [f], Glenn J. MacPherson [g], Julie Paque-Heather [h], David Wark [i,†]

[a] *Hawai'i Institute of Geophysics and Planetology, School of Ocean and Earth Science and Technology, University of Hawai'i at Manoa, Honolulu, HI 96822, USA*
[b] *Department of Earth and Planetary Sciences, Tokyo Institute of Technology, Meguro, Tokyo 152-8551, Japan*
[c] *Lawrence Livermore National Laboratory, Livermore, CA 94451, USA*
[d] *Centre de Recherches Pétrographiques et Géochimiques, CNRS-UPR 2300, BP20, 54501 Vandoeuvre les Nancy, France*
[e] *Ecole Nationale Supérieure de Géologie, INPL, BP40, 54501 Vandoeuvre les Nancy, France*
[f] *Harvard-Smithsonian Center for Astrophysics and Department of Earth and Planetary Sciences, Harvard University, Cambridge, MA 02138, USA*
[g] *Smithsonian Institution, Department of Mineral Sciences, NHB 119, Washington, DC 20560, USA*
[h] *Division of Geological and Planetary Sciences, California Institute of Technology, Pasadena, CA 91125, USA*
[i] *Earth Sciences, University of Melbourne, Parkville 3010, Australia*

Received 14 August 2006; accepted in revised form 5 March 2007; available online 16 June 2007

Abstract

The coarse-grained, igneous, anorthite-rich (Type C) CAIs from Allende studied (*100*, *160*, *6-1-72*, *3529-40*, *CG5*, *ABC*, *TS26*, and 93) have diverse textures and mineralogies, suggesting complex nebular and asteroidal formation histories. CAIs *100*, *160*, *6-1-72*, and *3529-40* consist of Al,Ti-diopside (fassaite; 13–23 wt% Al_2O_3, 2–14 wt% TiO_2), Na-bearing åkermanitic melilite (0.1–0.4 wt% Na_2O; $Åk_{30–75}$), spinel, and fine-grained (~5–10 μm) anorthite groundmass. Most of the fassaite and melilite grains have "lacy" textures characterized by the presence of abundant rounded and prismatic inclusions of anorthite ~5–10 μm in size. Lacy melilite is pseudomorphed to varying degrees by grossular, monticellite, and pure forsterite or wollastonite. CAI *6-1-72* contains a relict Type B CAI-like portion composed of polycrystalline gehlenitic melilite ($Åk_{10–40}$), fassaite, spinel, perovskite, and platinum-group element nuggets; the Type B-like material is overgrown by lacy melilite and fassaite. Some melilite and fassaite grains in CAIs *100* and *160* are texturally similar to those in the Type B portion of *6-1-72*. CAIs *ABC* and *TS26* contain relict chondrule fragments composed of forsteritic olivine and low-Ca pyroxene; CAI *93* is overgrown by a coarse-grained igneous rim of pigeonite, augite, and anorthitic plagioclase. These three CAIs contain very sodium-rich åkermanitic melilite (0.4–0.6 wt% Na_2O; $Åk_{63–74}$) and Cr-bearing Al,Ti-diopside (up to 1.6 wt% Cr_2O_3, 1–23 wt% Al_2O, 0.5–7 wt% TiO_2). Melilite and anorthite in the Allende Type C CAI peripheries are replaced by nepheline and sodalite, which are crosscut by andradite-bearing veins; spinel is enriched in FeO. The CAI fragment *CG5* is texturally and mineralogically distinct from other Allende Type Cs. It is anorthite-poor and very rich in spinel poikilitically enclosed by Na-free gehlenitic melilite ($Åk_{20–30}$), fassaite, and anorthite; neither melilite nor pyroxene have lacy textures; secondary minerals are absent. The Al-rich chondrules *3655b-2* and *3510-7* contain aluminum-rich and ferromagnesian portions. The Al-rich portions consist of anorthitic plagioclase, Al-rich low-Ca pyroxene, and Cr-bearing spinel; the ferromagnesium portions consist of fosteritic olivine, low-Ca pyroxene, and opaque nodules.

* Corresponding author. Fax: +1 808 956 6322.
E-mail address: sasha@higp.hawaii.edu (A.N. Krot).
† Deceased.

0016-7037/$ - see front matter © 2007 Published by Elsevier Ltd.
doi:10.1016/j.gca.2007.03.040

We conclude that Type C CAIs *100*, *160*, *6-1-72*, and *3529-40* formed by melting of coarse-grained Type B-like CAIs which experienced either extensive replacement of melilite and spinel mainly by anorthite and diopside (traces of secondary Na-bearing minerals, e.g., nepheline or sodalite, might have formed as well), or addition of silica and sodium during the melting event. *CG5* could have formed by melting of fine-grained spinel-melilite CAI with melilite and spinel partially replaced anorthite and diopside. CAIs *ABC*, *93*, and *TS-26* experienced melting in the chondrule-forming regions with addition of chondrule-like material, such as forsteritic olivine, low-Ca pyroxene, and high-Ca pyroxene. Anorthite-rich chondrules formed by melting of the Al-rich (Type C CAI-like) precursors mixed with ferromagnesian, Type I chondrule-like precursors. The Allende Type C CAIs and Al-rich chondrules experienced fluid-assisted thermal metamorphism, which resulted in pseudomorphic replacement of melilite and anorthite by grossular, monticellite, and forsterite (*100*, *160*, *6-1-72*, *3592-40*) or by grossular, monticellite, and wollastonite (*ABC*, *93*, *TS-26*). The pseudomorphic replacement was followed or accompanied by iron–alkali metasomatic alteration resulting in replacement of melilite and anorthite by nepheline and sodalite, enrichment of spinel in FeO, and precipitation of salite–hedenbergite pyroxenes, wollastonite, and andradite in fractures and pores in and around CAIs.
© 2007 Published by Elsevier Ltd.

1. INTRODUCTION

Coarse-grained, igneous, anorthite-rich (Type C) CAIs were initially recognized in the Allende meteorite (Wark, 1987; Beckett and Grossman, 1988; Imai and Yurimoto, 2000), and subsequently described in the CR (Aléon et al., 2002; Krot et al., 2005a), CO (Itoh et al., 2004), and anomalous carbonaceous chondrites Ningqiang (CV/CK-like) (Lin and Kimura, 1998, 2003; Kita et al., 2004), Acfer 094 (CO/CM-like) (Krot et al., 2004a), and Isheyevo (CH/CB-like) (Krot et al., 2006a). Type C CAIs consist of Al,Ti-diopside (fassaite), spinel, melilite, and abundant anorthite. When projected from spinel onto the gehlenite–anorthite–forsterite plane in the $CaO–MgO–A_2O_3–SiO_2$ system (Stolper, 1982), their spinel-saturated, bulk compositions plot in the liquidus field of anorthite (Fig. 1EA) and define a linear trend toward compositions of Type A and B CAIs, which on the same projection plot in the liquidus field of melilite (Beckett and Grossman, 1988). Bulk chemical compositions of Type C CAIs are similar to those of fine-grained, spinel-, anorthite-rich inclusions, providing a potential link between these CAI types (Lin and Kimura, 1998; Krot et al., 2004b). They are also similar to bulk compositions of some Al-rich chondrules (>10 wt% Al_2O_3; Bischoff and Keil, 1984) from carbonaceous chondrites (Krot and Keil, 2002; Krot et al., 2002; MacPherson and Huss, 2005) providing a potential link between CAIs and that type of chondrules (Beckett and Grossman, 1988). The latter is consistent with the observations that (i) most relict CAIs inside Al-rich chondrules consist of anorthite, spinel, and diopside (e.g., Krot and Keil, 2002; Krot et al., 2002, 2004a), and (ii) some Type C CAIs from CV and CR chondrites experienced a late-stage melting event(s) with or without addition of chondrule material, and oxygen isotopic exchange with an ^{16}O-poor nebular gas (Krot et al., 2005a,b, 2007a,b), probably in the chondrule-forming region.

In order to understand the origin of Type C CAIs in carbonaceous chondrites and their possible genetic relationship to other types of refractory inclusions and Al-rich chondrules, we initiated a detailed study of their mineralogy, petrography, trace element contents, oxygen and aluminum–magnesium isotopic compositions. The preliminary studies of trace element abundances and oxygen isotopic compositions have been described by Huss et al. (2002) and Krot et al. (2007b). Here, we report the mineralogy and petrography of five Type C CAIs from Allende: *100*, *160*, *CG5*, *6-1-72*, and *3529-40*, and two Al-rich chondrules (*3510-7* and *3555B-2*), and compare them with our recent results on three chondrule-bearing Type C CAIs from Allende *ABC*, *93*, and *TS26* (Krot et al., 2005b, 2007b). Although most of the Allende Type C CAIs described here have been previously studied by Wark (1987), we think that some important aspects of their formation have been overlooked. The preliminary results of this study have been reported by Krot et al. (2004c).

2. ANALYTICAL PROCEDURES

Polished thin and thick sections of the Allende Type C CAIs *100*, *160*, *CG5*, *6-1-72*, *3529-40*, *ABC*, *TS26*, and *93*, and two Al-rich chondrules *3510-7* and *3555B-2* (Table 1) were studied using optical microscopy, X-ray elemental mapping, backscattered electron (BSE) imaging, and electron probe microanalysis (EPMA). The BSE images and semi-quantitative analyses were obtained with the JEOL JSM-5900LV scanning electron microscope equipped with

Table 1
List of the Allende Type C CAIs and Al-rich chondrules studied

Object, #	Ref.
Type C CAIs	
CG5	Wark (1987)
With lacy melilite and fassaite	
100	Wark (1987)
160	Wark (1987)
6-1-72	Wark (1987)
3529-40	Wark (1987)
With chondrule-like material	
ABC	Wark (1987), MacDougall et al. (1981), Krot et al. (2005b), Krot et al. (2007a)
TS26	Wark (1987), Krot et al. (2005b), Krot et al. (2007a)
93	Wark (1987), Krot et al. (2005b), Krot et al. (2007a)
Al-rich chondrules	
3655b-2	Wark (1987)
3510-7	Wark (1987)

Thermo Electron energy dispersive spectrometer (EDS) using a 15–20 kV accelerating voltage and 1–2 nA beam current. Some of the sections were previously Au-coated. Because the sections are old, we made no attempts to remove traces of Au, which resulted in appearances of bright white spots in BSE images. X-ray elemental maps with a resolution of 1–10 μm/pixel were acquired using five spectrometers of a Cameca SX-50 microprobe at 15 keV accelerating voltage, 50–100 nA beam current and ~1–2 μm beam size. The elemental maps in Mg, Ca, and Al Kα were combined using a RGB-color scheme and Environment for Visualizing Images (ENVI) software package.

Electron probe microanalyses were performed with a Cameca SX-50 electron microprobe using a 15 keV accelerating voltage, 10–20 nA beam current, beam size of ~1–2 μm and wavelength dispersive X-ray spectrometry. For each element, counting times on both peak and background were 30 s (10 s for Na and K). Bulk compositions of chondrules were measured using a defocused ~10-μm beam. Matrix effects were corrected using the PAP procedure. The detection limits were (in wt%): SiO_2, Al_2O_3, MgO, CaO, 0.03; TiO_2, Cr_2O_3, 0.04; K_2O, 0.04; Na_2O, 0.06; MnO, FeO, 0.07.

3. RESULTS

CAI fragment *CG5* is composed of lath-shaped anorthite, fassaite and melilite, all poikilitically enclosing abundant spinel grains; secondary minerals and Wark-Lovering rim layers are absent (Fig. 1). Melilite and pyroxene occur in interstitial regions between prismatic anorthite crystals; they also form large, massive grains in the anorthite-poor regions of the CAI. Pyroxene has high Al_2O_3 (up to 21 wt%) and TiO_2 contents (up to 8 wt%); (Fig. 2) calculations of structural formula of pyroxene revealed no Ti^{3+} (Table 2). Melilite is Åk-poor (9–26 mol%); Na contents are generally below the detection limit of the electron microprobe (Table 3 and Fig. 3). Spinel and anorthite are nearly pure $MgAl_2O_4$ and $CaAl_2Si_2O_8$, respectively (Tables 1EA and 2EA).

Our sample of CAI *100* consists of four fragments (hereafter, "*100a*", "*100b*", "*100c*", and "*100d*"). The petrographic context of the fragments is unknown, and none of them have Wark-Lovering rim layers (Fig. 4). In addition, secondary Fe- or alkali-rich minerals (nepheline, sodalite, andradite, and hendenbergite) that are commonly observed around peripheries of Allende CAIs are nearly absent. Based on these observations, we infer that these fragments probably represent the core and/or mantle of the original, unbroken CAI. There are significant variations in the morphology of Al,Ti-diopside and melilite grains and distribution of spinel among the fragments (Figs. 4 and 5). Below we describe in detail only the mineralogy of *100a*; for other fragments, we summarize the features which could be important for understanding the genesis of the inclusion.

Fragment *100a* consists of coarse, euhedral-to-subhedral grains of fassaite, melilite, spinel, and fine-grained (~5 μm in size) anorthite groundmass (Fig. 4a). Melilite grains typically contain abundant inclusions of anorthite (this texture

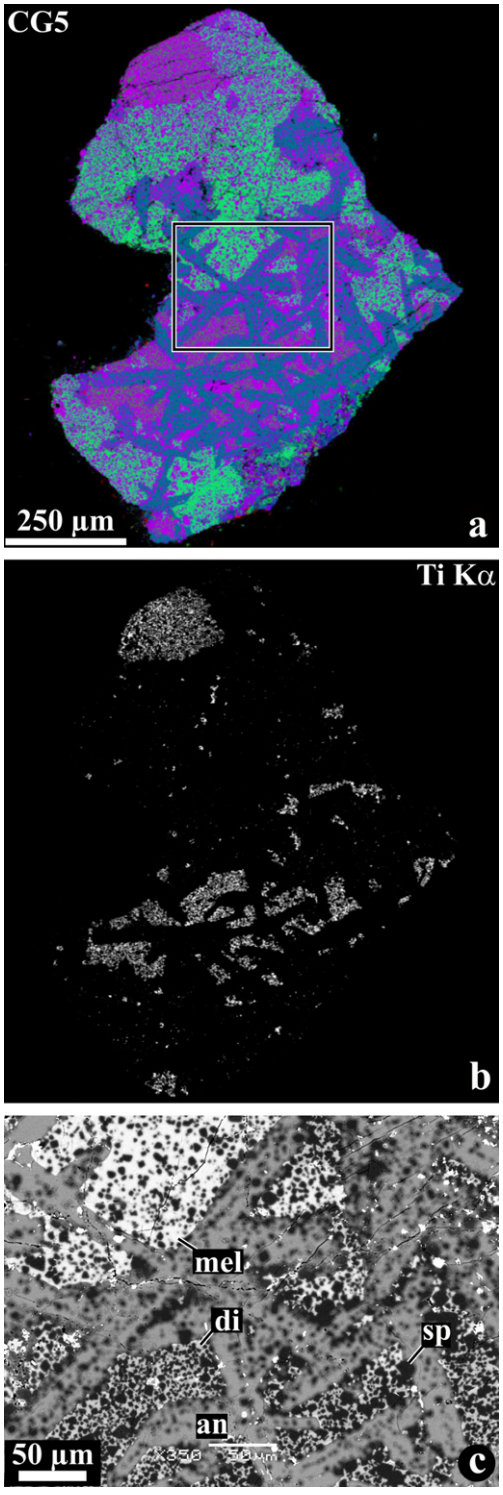

Fig. 1. (a) Combined elemental map in Mg (red), Ca (green), and Al Kα (red) X-rays, (b) elemental map in Ti Kα and (c) BSE image of a Type C CAI fragment *CG5*. The region outlined in (a) is shown in detail in (b). The CAI consists of lath-shaped anorthite with interstitial fassaite (Al,Ti-diopside) and melilite; melilite and fassaite also anorthite-poor massive regions. All minerals poikilitically enclose numerous spinel grains. Bright white spots in (c) are gold left after coating. an, anorthite; mel, melilite; di, fassaite; sp, spinel.

Table 2
Electron microprobe analyses (in wt%) of pyroxenes in the Allende Type C CAIs and Al-rich chondrules

Object, # location	3529-40				6-1-72					100			CG5	160				3510-7			3555B-2		
	Core	Core	Rim	Rim	Type C		Type B			Core			Core	Core		Mantle		px	px	px	cpx	opx	px
SiO_2	39.6	33.7	52.8	50.6	37.2	33.5	37.9	34.0	32.3	45.4	41.3	24.8	35.6	41.6	39.6	36.8	34.7	54.6	49.3	49.6	52.9	58.0	56.0
TiO_2	7.2	10.9	<0.04	0.11	8.0	13.7	7.7	11.9	16.3	2.3	5.7	12.7	7.9	4.6	6.6	9.2	13.9	0.94	3.6	1.4	1.5	0.32	0.58
TiO_2	3.8	6.7	—	0.11	5.0	5.3	1.2	5.1	2.1	1.3	2.0	7.1	7.9	1.3	2.4	4.0	3.2	0.94	1.2	0.92	0.46	0.32	0.58
Ti_2O_3	3.0	3.8	—	0.00	2.7	7.5	5.9	6.1	12.7	0.90	3.3	5.0	0.01	3.0	3.8	4.6	9.6	0.00	2.2	0.45	0.92	—	—
Al_2O_3	17.2	22.5	1.7	5.2	19.1	20.9	21.4	21.5	20.3	13.3	17.6	33.1	20.9	17.8	19.2	19.4	19.5	3.5	12.6	13.8	2.7	1.1	2.2
Cr_2O_3	0.08	0.12	0.08	0.14	0.16	0.11	0.15	0.16	0.30	0.07	0.12	0.39	0.08	0.08	0.11	0.11	0.08	0.42	0.56	0.64	0.63	0.43	0.73
FeO	<0.07	<0.07	0.13	0.07	<0.07	<0.07	<0.07	<0.07	<0.07	<0.07	<0.07	<0.07	<0.07	<0.07	<0.07	0.14	<0.07	1.2	0.18	0.19	0.42	0.52	0.52
MnO	<0.07	<0.07	<0.07	<0.07	<0.07	<0.07	<0.07	<0.07	<0.07	<0.07	<0.07	<0.07	<0.07	<0.07	<0.07	<0.07	<0.07	0.11	<0.07	<0.07	<0.07	<0.07	<0.07
MgO	10.5	8.0	17.9	16.7	9.3	6.9	8.2	7.2	5.3	12.8	10.3	2.5	11.4	10.7	9.8	8.8	7.2	35.5	33.2	33.3	23.5	38.6	36.7
CaO	24.9	25.1	25.8	26.0	25.4	25.4	24.8	25.2	24.4	25.5	25.6	24.7	22.9	24.8	24.9	24.9	24.8	3.0	0.51	0.39	16.7	0.51	2.3
Total	99.1	99.8	98.5	98.8	98.8	99.8	99.5	99.3	97.4	99.3	100.3	97.6	98.9	99.3	99.9	98.8	99.1	99.2	99.6	99.3	98.3	99.5	99.0
Structural formulae, based on 6 [O]																							
Si	1.470	1.258	1.941	1.857	1.394	1.263	1.405	1.279	1.258	1.662	1.513	0.957	1.321	1.531	1.457	1.382	1.318	1.878	1.679	1.685	1.907	1.962	1.919
Al(IV)	0.530	0.742	0.059	0.143	0.606	0.737	0.595	0.721	0.742	0.338	0.487	1.043	0.679	0.469	0.543	0.618	0.682	0.122	0.321	0.315	0.093	0.038	0.081
Ti^{4+}	0.106	0.188	0.000	0.003	0.141	0.151	0.034	0.145	0.063	0.037	0.054	0.205	0.220	0.035	0.067	0.114	0.093	0.024	0.030	0.023	0.012	0.008	0.015
Ti^{3+}	0.094	0.117	0.000	0.000	0.085	0.237	0.182	0.192	0.414	0.027	0.102	0.161	0.000	0.093	0.116	0.144	0.304	0.000	0.062	0.013	0.028	0.000	0.000
Al(VI)	0.222	0.246	0.016	0.081	0.235	0.193	0.340	0.234	0.189	0.235	0.274	0.459	0.236	0.303	0.291	0.242	0.188	0.018	0.185	0.238	0.023	0.006	0.007
Fe	0.000	0.000	0.004	0.002	0.000	0.000	0.000	0.000	0.000	0.000	0.000	0.000	0.000	0.000	0.000	0.004	0.000	0.034	0.005	0.006	0.013	0.015	0.015
Mn	0.000	0.000	0.000	0.000	0.000	0.000	0.000	0.000	0.000	0.000	0.000	0.000	0.000	0.000	0.000	0.000	0.000	0.003	0.000	0.000	0.000	0.000	0.000
Cr	0.002	0.004	0.002	0.004	0.005	0.003	0.004	0.005	0.009	0.002	0.004	0.012	0.002	0.002	0.003	0.003	0.002	0.011	0.015	0.017	0.018	0.012	0.020
Mg	0.583	0.443	0.982	0.914	0.517	0.389	0.455	0.406	0.308	0.700	0.562	0.144	0.630	0.588	0.539	0.491	0.407	1.819	1.685	1.688	1.263	1.943	1.871
Ca	0.993	1.002	1.016	1.022	1.017	1.026	0.984	1.018	1.020	0.999	1.005	1.018	0.911	0.978	0.984	1.000	1.006	0.112	0.019	0.014	0.644	0.018	0.084
Total	4.000	4.000	4.020	4.026	4.000	4.000	4.000	4.000	4.002	4.000	4.000	4.000	4.000	4.000	4.000	4.000	4.001	4.022	4.000	4.000	4.000	4.002	4.012

Na_2O and K_2O are below the detection limits (<0.06 and 0.04 wt%, respectively).

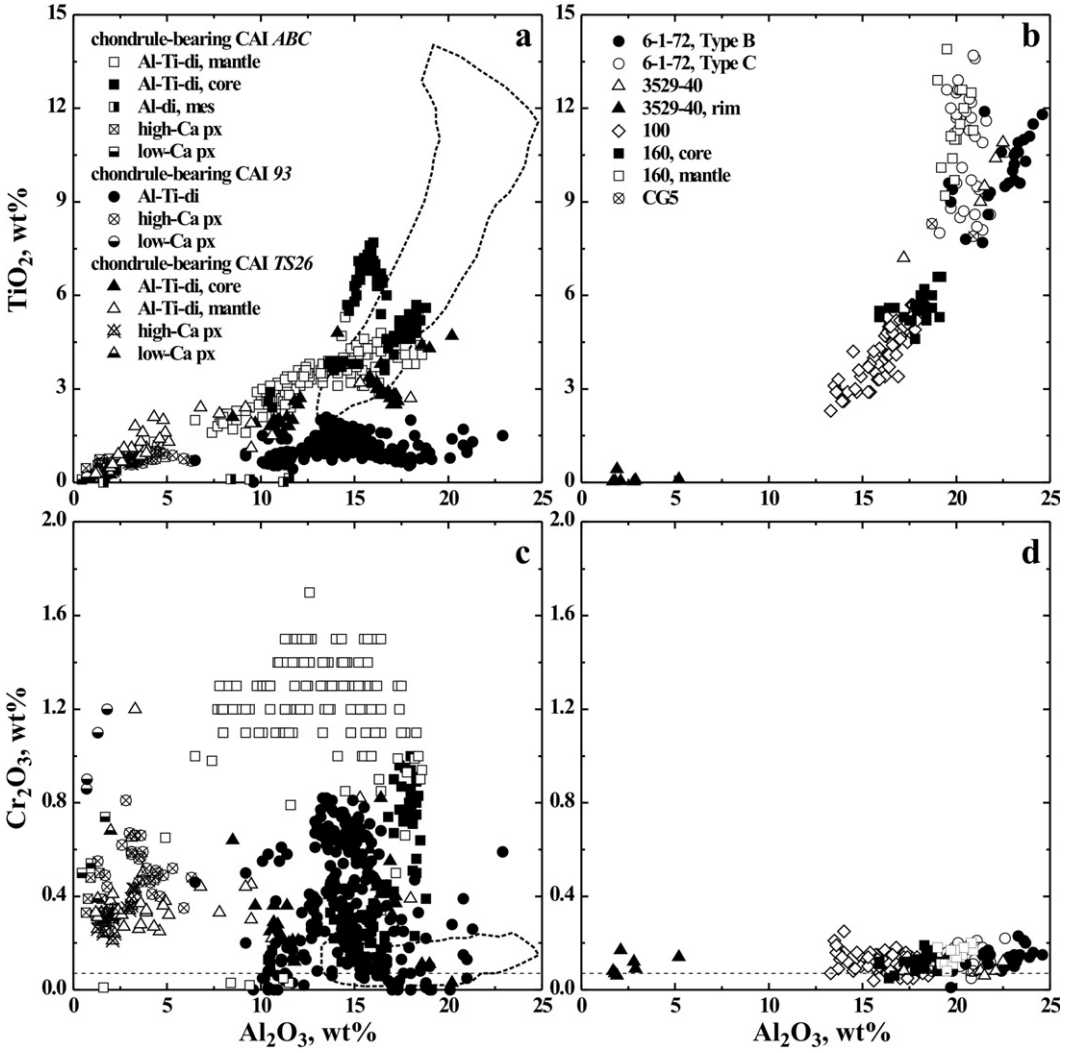

Fig. 2. (a) Cr_2O_3 *vs.* Al_2O_3 and (b) TiO_2 *vs.* Al_2O_3 (in wt%) in pyroxenes of Type C CAIs with (a and c) and without (b and d) chondrule material; fields occupied by the latter are outlined in (a) and (c). Compositions of pyroxenes from the chondrule-bearing Type C CAIs *ABC*, *TS26*, and *93* are from Krot et al. (2007a).

Table 3
Electron microprobe analyses (in wt%) of melilite in the Allende Type C CAIs

CAI, #	*3529-40*		*100*	*100*	*CG5*	*CG5*	*160*, c	*160*, c	*160*, m	*160*, m	*6-1-72,*	Type C	*6-1-72,*	Type B
SiO_2	28.9	30.9	35.0	38.8	24.4	27.2	34.7	37.6	31.8	34.5	29.5	34.8	23.2	30.6
TiO_2	0.05	<0.04	<0.04	<0.04	0.06	0.06	<0.04	0.04	0.05	0.07	<0.04	<0.04	0.09	<0.04
Al_2O_3	25.2	22.2	16.4	10.2	33.8	26.2	15.3	10.1	20.6	15.6	25.2	18.2	35.5	23.4
Cr_2O_3	<0.04	0.05	<0.04	<0.04	<0.04	<0.04	<0.04	0.07	<0.04	<0.04	<0.04	<0.04	<0.04	<0.04
FeO	<0.07	<0.07	<0.07	<0.07	<0.07	<0.07	0.46	<0.07	<0.07	<0.07	<0.07	<0.07	<0.07	<0.07
MnO	<0.07	<0.07	<0.07	<0.07	0.09	0.07	<0.07	<0.07	0.07	<0.07	<0.07	<0.07	<0.07	<0.07
MgO	4.8	6.1	8.0	10.3	4.8	4.0	<0.07	10.5	6.4	8.2	4.6	7.3	0.79	5.4
CaO	40.6	40.4	39.8	40.7	37.8	40.9	40.0	40.2	40.1	40.4	40.2	39.4	40.3	40.0
Na_2O	0.12	0.13	0.19	0.17	<0.06	<0.06	0.36	0.11	0.32	0.33	0.19	0.33	<0.06	0.17
Total	99.7	99.8	99.4	100.2	101.0	98.4	90.8	98.7	99.3	99.2	99.7	100.0	99.9	99.5
Ak	32	41	58	74	9	26	56	72	44	56	33	54	5	38

c, core; m, mantle.

was called ''lacy'' or ''eutectic'' by Wark, 1987); anorthite-free, massive melilite regions are rare and overgrown by lacy melilite (Fig. 5a–c). Lacy melilite grains are pseudomorphed to varying degrees by grossular ($Ca_3Al_2Si_3O_{12}$),

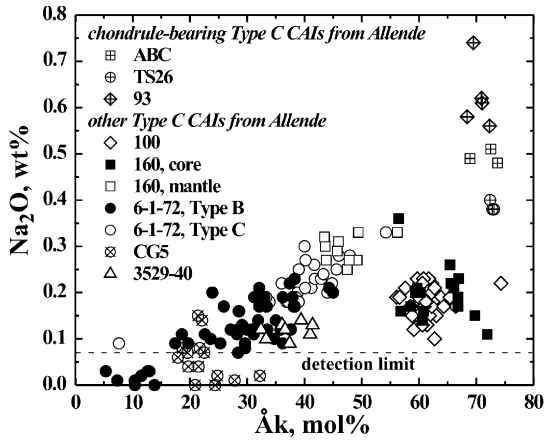

Fig. 3. Åkermanite (mol%) *vs.* Na_2O (wt%) contents in melilite of the Allende Type C CAIs. Compositions of melilite from the chondrule-bearing Type C CAIs *ABC*, *TS26*, and *93* are from Krot et al. (2007a).

monticellite ($CaMgSiO_4$), and pure forsterite (Mg_2SiO_4) (Fig. 5a–d). Although the outlines of the original melilite grains are generally well-preserved, the replaced portions are highly porous, suggesting volume change during the replacement. Grossular occurs as anhedral or subhedral grains closely associated with monticellite and forsterite (Tables 4 and 5). Forsterite commonly occurs as anhedral and subhedral grains between grossular grains (Fig. 5e and f). X-ray elemental mapping reveals enrichment in Na along the peripheries of the pseudomorphed portions of the melilite grains (Fig. 2EA). This enrichment is associated with numerous, tiny pores surrounding the replaced portions of the grains (Fig. 5e and f). Because no alkali-rich phases have been observed, it seems possible that Na is concentrated in a thin layer of the surrounding anorthite. Fassaite occurs as isolated grains or as intergrowths with melilite and spinel framboids in the anorthite groundmass (Fig. 5b and c). Cores of the coarse fassaite grains contain abundant, rounded inclusions of anorthite, and are surrounded by compact, inclusion-poor layers that have very irregular (possibly corroded) peripheries (Fig. 5b and c). Spinel occurs as framboids, aggregates of grains and isolated grains in anorthite, pyroxene and melilite. The spinel framboids commonly enclose inclusions of melilite, fassaite, and anorthite.

Fragment *100b* has two texturally distinct portions (Fig. 4b). Its left portion is texturally and mineralogically similar to the fragment *100a* and contains coarse (100–200 μm in size), euhedral fassaite grains with lacy textures. The right portion in Fig. 4b contains abundant, small (20–30 μm in apparent diameter) fassaite crystals, which are nearly free of anorthite inclusions (Fig. 5j). Melilite grains are extensively replaced by grossular, monticellite, and forsterite (Fig. 5e and f). Spinel grains occur mainly as aggregates, framboids, and as inclusions in melilite and pyroxene; isolated spinel grains in anorthite are relatively rare.

Fragments *100c* and *100d* consist of the same minerals as two other fragments, but contain mostly only one textural type of fassaite—small, euhedral grains (Figs. 4c,d and 5i). In addition, there is a compact aggregate of chemically zoned fassaite grains, which has an irregular (possibly corroded) outline (Figs. 5g,h and 3EA). Isolated spinel grains are ubiquitous in the anorthite groundmass.

There is no correlation between the morphological types of fassaite and their compositions; they contain 13–18 wt% Al_2O_3 and 2–6 wt% TiO_2. One of the fassaite grains is highly enriched in Al_2O_3 (33 wt%) and TiO_2 (13 wt%) and could be either relict or a product of dissolution of perovskite in the CAI melt (Lin et al., 2003) (Table 2 and Fig. 2). Melilite is Na- and Åk-rich ($Ak_{58–74}$, 0.15–0.25 wt% Na_2O; Table 3, Fig. 3). Anorthite and spinel are nearly pure $CaAl_2Si_2O_8$ (Table 1EA) and $MgAl_2O_4$ (Table 2EA), respectively.

CAI *6-1-72* is a complete, ellipsoid inclusion surrounded by a Wark-Lovering rim sequence of spinel, fassaite, and olivine (Fig. 6). It consists of two texturally distinct regions, easily recognizable in a Ca Kα X-ray map (Fig. 6c). Its main portion is mineralogically similar to the other Allende Type C CAIs described above and consists of fine-grained groundmass anorthite and coarse-grained, lacy fassaite and melilite; spinel is relatively minor and heterogeneously distributed in the CAI (Figs. 6 and 7). Coarse melilite–anorthite grains are pseudomorphed by a fine-grained, porous mixture of grossular, monticellite, and forsterite. The groundmass anorthite contains anhedral intergranular fassaite grains; their abundance increases towards the CAI periphery. The CAI core is free of nepheline and sodalite; both minerals, however, are common in the CAI periphery, where they replace anorthite and, possibly, melilite (Figs. 6d and 7). Nepheline, sodalite, and grossular–monticellite–forsterite pseudomorphs are crosscut by andradite-bearing veins (Fig. 7). The CAI core is heavily fractured; some of the fractures are filled by andradite and wollastonite (Fig. 7f).

The right portion of *6-1-72* in Fig. 6 is texturally and mineralogically similar to Type B inclusions from CV chondrites (e.g., MacPherson et al., 1988). It consists of compact, polycrystalline melilite, fassaite, isolated spinel grains, and a spinel palisade body (Figs. 8 and 9). Melilite and fassaite contain abundant inclusions of spinel, perovskite, and platinum group element nuggets; neither melilite nor fassaite have lacy texture. Melilite along grain boundaries is replaced by a fine-grained mixture of grossular, monticellite, and forsterite. Coarse-grained melilite and the palisade body in the Type B-like portion are overgrown by lacy fassaite (Fig. 9b–d).

Pyroxenes in both portions of the CAI are compositionally similar and have high Al_2O_3 (19–21 wt%) and TiO_2 (8–16 wt%) contents (Table 2 and Fig. 2). Melilite grains show wide compositional variations, with those of the Type C portion being enriched in Åk (33–54 mol%) and Na_2O (0.19–0.33 wt%) relative to those of the Type B portion (5–38 mol% and <0.17 wt%, respectively) (Table 3 and Fig. 3). Anorthite is nearly pure $CaAl_2Si_2O_8$ (Table 1EA). Spinel in the CAI core is nearly pure $MgAl_2O_4$; spinel of the Wark-Lovering rim is enriched in FeO (based on the semi-quantative EDS analyses).

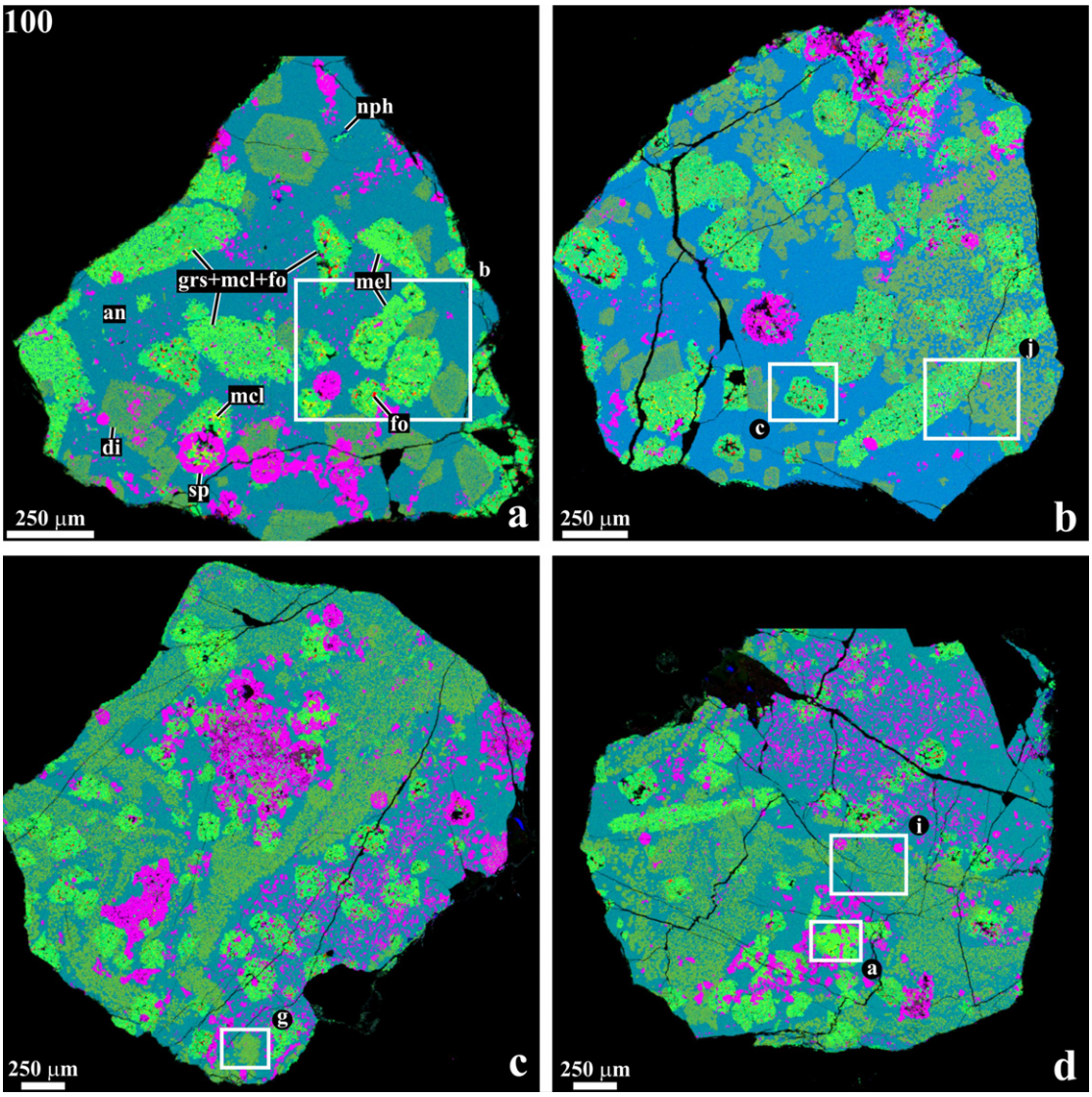

Fig. 4. Combined elemental maps in Mg (red), Ca (green), and Al Kα (blue) X-rays of the four fragments (a–d) of Type C CAI *100*. Regions outlined and labeled in (a) are shown in detail in Fig. 5. The CAI is composed of fassaite, melilite, and spinel surrounded by anorthite groundmass. Lacy melilite grains are almost completely pseudomorphed by grossular, monticellite, and forsterite (see Fig. 5 for details). Secondary nepheline replacing melilite is very minor. Spinel occurs in palisade bodies, as aggregates of grains and as isolated incusions in anorthite, pyroxene, and melilite. There are significant variations in modal mineralogy and morphology of the pyroxene, melilite, and spinel grains among the fragments (see text for details). fo, forsterite; grs, grossular; mtc, monticellite; nph, nepheline.

CAI *160* is a fragmented inclusion partly surrounded by spinel, Al,Ti-diopside, and olivine rims (Fig. 10). It is composed of fassaite, melilite, spinel, and a very fine-grained anorthite groundmass (Fig. 11a and b). Melilite and anorthite in the outer portion of the CAI and along the fractures in the core are replaced by nepheline and sodalite (Fig. 10c and d). Fassaite occurs as lacy grains (Fig. 11c and d), as rare massive grains poikilitically enclosing euhedral spinel (Fig. 11e), and as interstitial grains between polycrystalline melilite (Fig. 11f). The outer portions of the massive pyroxene grains contain abundant inclusions of anorthite. Pyroxenes in the CAI core contain lower TiO_2 contents than those in its mantle (4.6–6.6 *vs.* 9.2–13.9 wt%); both occurrences have high Al_2O_3 (18–20 wt%) (Table 2 and Fig. 2). There are no compositional differences between the massive and lacy pyroxenes.

Melilite occurs as coarse, subhedral grains with abundant inclusions of anorthite (Fig. 11c and d) and as compact polycrystalline regions with interstitial fassaite (Fig. 11f). The melilite grains with anorthite inclusions are pseudomorphed to varying degrees by a porous, fine-grained mixture of grossular, monticellite, and forsterite (Fig. 11c and d). The polycrystalline melilite regions are texturally similar to those in the Type B-like portion of the CAI *6-1-72* (Fig. 9e and f); they are only slightly

replaced by grossular, monticellite, and forsterite along the grain boundaries. The interstitial fassaite in these regions contains abundant inclusions of anorthite (Fig. 11f). Melilite in the CAI mantle is more gehlenitic than in its core (44–56 *vs.* 56–72 mol%); in both occurrences, melilite contains high Na_2O contents (up to 0.36 wt%) (Table 3 and Fig. 3).

Anorthite in the center of the CAI is nearly free of small inclusions of fassaite (Fig. 11c); anorthite in the CAI mantle contains abundant inclusions of anhedral fassaite which

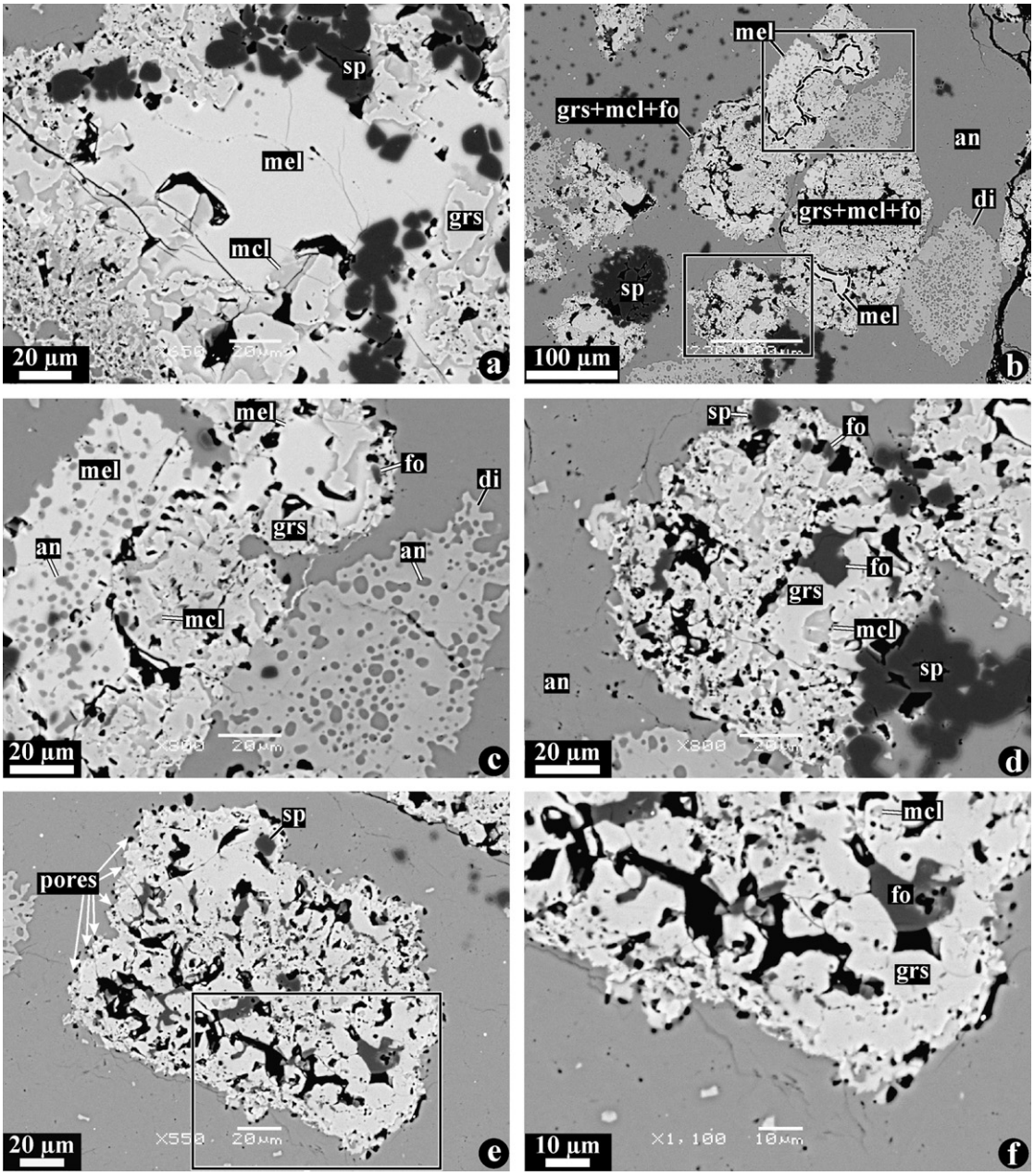

Fig. 5. BSE images of a Type C CAI *100*. Regions outlined in (b) (top and bottom) are shown in details in (c) and (d), respectively. Regions outlined in (e) and (g) are shown in detail in (f) and (h), respectively. Lacy melilite grains are pseudomorphed by grossular, monticellite, and forsterite to various degrees; thin veins of grossular identified by EDS only crosscutting anorthite are very rare (c). The relict melilite regions (outlined in b and j) appear to be corroded by the surrounding anorthite and contain abundant inclusions of anorthite (b, c, and j); occasionally, relict melilite occurs as massive grains free of anorthite inclusions (a). The pseudomorphed regions of melilite are highly porous and contain subhedral inclusions of grossular and forsterite (d and f). Abundant pores are also observed along the boundaries between the pseudomorphed melilite regions and groundmass anorthite (e). Coarse pyroxene grains appear to be corroded by anorthite and contain abundant inclusions of anorthite (b and c). Small pyroxene grains are nearly free of anorthite inclusions (i and j). Occasionally, pyroxene grains form compact aggregates resorbed by anorthite around the peripheries; pyroxene aggregates show compositional variations (can be seen as variations in brightness; darker regions are indicated in (h) by short double lines; AB indicates compositional profile shown in Fig. 3EA).

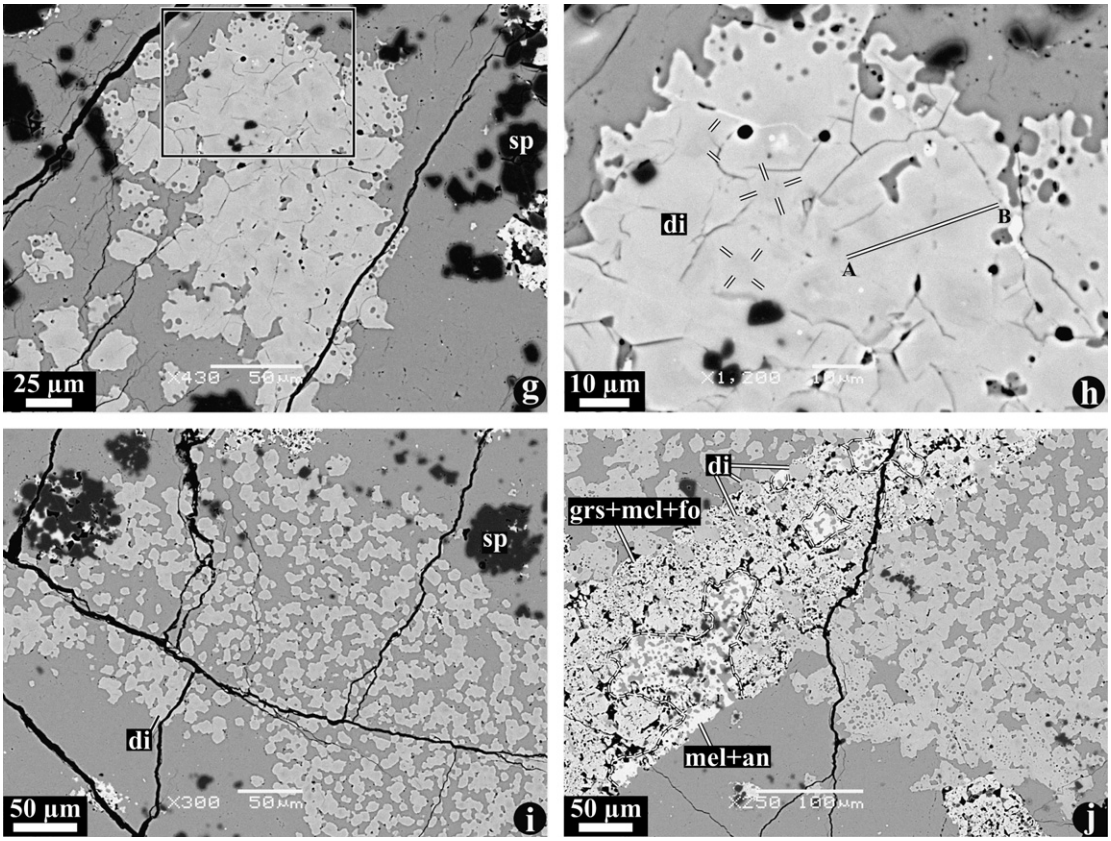

Fig. 5 (*continued*)

Table 4
Electron microprobe analyses (in wt%) of olivine in the Allende Type C CAI and Al-rich chondrules

Object, #	*100*	*3510-7*		*3555B-2*
SiO_2	43.2	40.9	39.7	39.4
TiO_2	<0.04	0.17	0.11	0.05
Al_2O_3	<0.03	0.06	<0.03	0.41
Cr_2O_3	<0.04	0.08	<0.04	0.04
FeO	<0.07	0.26	9.2	13.5
MnO	<0.11	<0.07	0.12	0.11
MgO	57.0	56.9	50.2	45.1
CaO	0.37	0.12	0.13	0.14
Total	100.5	98.4	99.4	98.7
Fa	0	0.1	5.5	8.6

occupy interstitial regions between individual anorthite grains. Anorthite is compositionally pure $CaAl_2Si_2O_8$ (Table 1EA).

Spinel is heterogeneously distributed within the CAI and occurs as individual grains enclosed in melilite, anorthite and fassaite, and as framboids. In the CAI core and mantle, it is nearly pure $MgAl_2O_4$ (Table 2EA); spinel in the altered portion of the CAI, including the Wark-Lovering rim, is enriched in FeO (based on the EDS semi-quantitative analyses).

The CAI is surrounded by a fine-grained rim largely composed of ferrous olivine and nepheline. Compared to the neighboring matrix, the fine-grained rim is depleted in nodules composed of Ca,Fe-rich pyroxenes, andradite, and wollastonite (Fig. 12d). An embayment in the unrimmed portion of the CAI is filled by closely intergrown andradite, sodalite, wollastonite, and salite–hedenbergite pyroxenes (Fig. 12e and f). A CAI near this region is extensively replaced by nepheline and sodalite (Fig. 10c and d).

CAI *3529-40* is a fragmented inclusion composed of anorthite, fassaite, and melilite, all poikilitically enclosing isolated spinel grains (Figs. 4EA and 5EA). Fassaite (7–11 wt% TiO_2; 17–23 wt% Al_2O_3) and melilite ($Åk_{32-31}$; ~0.1 wt% Na_2O) occur as coarse, anhedral grains with abundant inclusions of anorthite and are often intergrown (Figs. 5a,bEA). Melilite is extensively pseudomorphed by a fine-grained porous material composed of grossular, monticellite, and forsterite (forsterite and monticellite are too fine-grained to be analyzed by electron microprobe, and were identified by EDS on SEM). In regions with large pores, grossular occurs as coarse, subhedral crystals (Figs. 5c,dEA). Some portions of the CAI are surrounded by layers of Ti-poor Al-diopside and andradite (Fig. 5eEA and Table 2), whereas others are rimmed only by spinel (Fig. 5fEA). Anorthite near the spinel layer (Fig. 5eEA) is replaced by nepheline; this spinel is enriched in FeO (Table 2EA). No alkali-rich phases were observed near the Al-diopside layer (Fig. 5fEA).

Table 5
Electron microprobe analyses (in wt%) of grossular, wollastonite, andradite, forsterite, monticellite, and nepheline in the Allende Type C CAIs and Al-rich chondrules

Object, # min	*100*					*160*	*3529-40*	*3510-7*		*3555B-2*
	mtc	mtc	grs	grs	nph	grs	grs	andr	nph	nph
SiO_2	38.1	37.7	40.3	41.4	37.0	39.8	39.0	46.8	42.3	41.8
TiO_2	<0.04	<0.04	<0.04	<0.04	<0.04	<0.04	0.06	<0.04	0.04	<0.04
Al_2O_3	0.13	2.6	22.8	22.2	34.0	23.9	24.2	0.24	36.7	37.7
Cr_2O_3	<0.04	<0.04	<0.04	<0.04	<0.04	<0.04	<0.04	<0.04	<0.04	<0.04
FeO	<0.07	<0.07	<0.07	<0.07	<0.07	<0.07	0.14	26.4	0.14	0.15
MnO	<0.07	<0.07	<0.07	<0.07	<0.07	<0.07	<0.07	1.3	<0.07	<0.07
MgO	25.5	23.8	0.58	2.7	0.08	1.1	0.89	0.06	0.03	0.08
CaO	35.1	35.5	35.9	35.3	5.8	36.7	35.8	22.8	2.2	2.0
Na_2O	<0.06	<0.06	<0.06	<0.06	23.2	<0.06	<0.06	<0.06	17.0	17.3
K_2O	<0.04	<0.04	<0.04	<0.04	<0.04	<0.04	<0.04	<0.04	1.6	1.5
Total	98.9	99.7	99.6	101.6	100.0	101.5	100.1	97.6	100.0	100.5

Chondrule *3510-7* (Fig. 13) consists of two, mineralogically distinct regions. Its main, Al-rich portion has a quench texture and is metal-free; it is composed of lath-shaped anorthitic plagioclase (An_{92-98}), Cr-bearing spinel (0.9 wt% Cr_2O_3), interstitial forsterite, Al-rich (13–14 wt% Al_2O_3) low-Ca pyroxene, and fine-grained mesostasis (Tables 2, 4, and Figs. 1EA, 2EA). Most of the mesostasis is replaced by hedenbergite (Fig. 13f). A small portion of

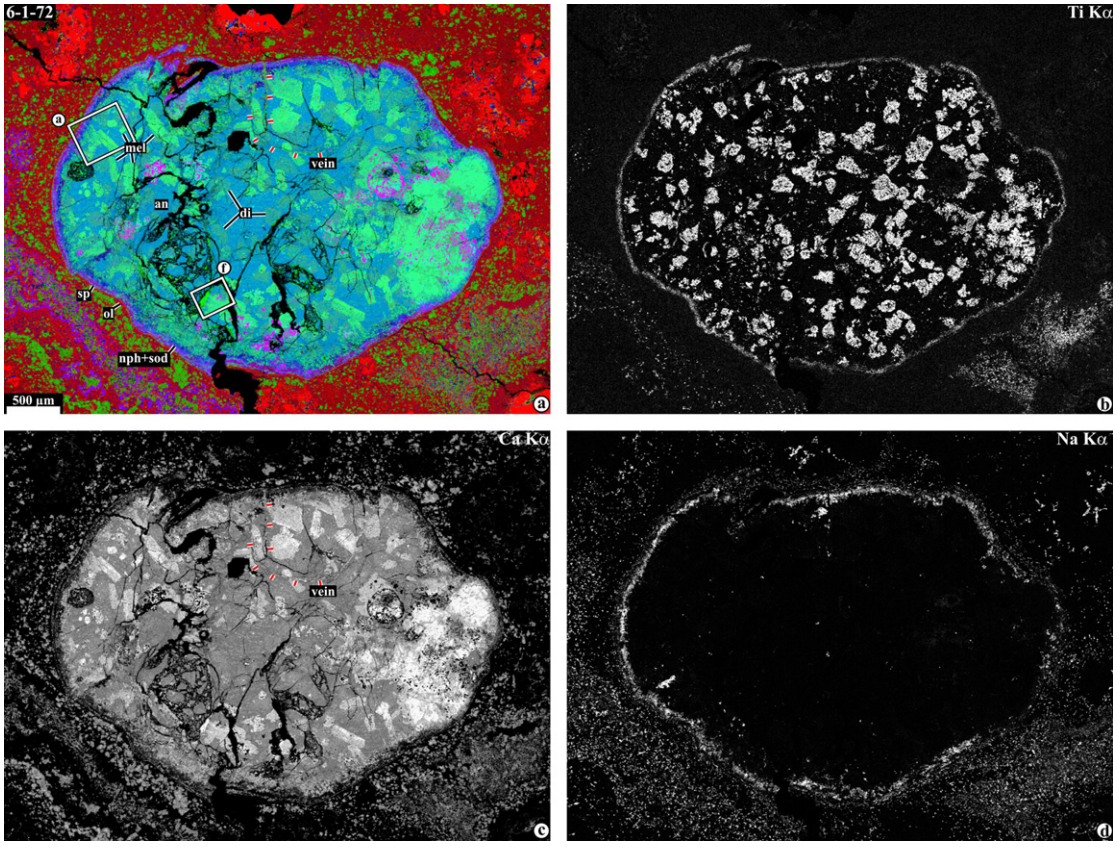

Fig. 6. Combined elemental map in Mg (red), Ca (green), and Al Kα (blue) X-rays (a), and elemental maps in Ti (b), Ca (c) and Na Kα (d) X-rays of the Allende CAI *6-1-72*. Regions outlined and labelled in (a) are shown in detail in Fig. 7. The CAI consists of two texturally and mineralogically distinct regions, easily recognizable in (c). Its main portion is mineralogically similar to Type C CAIs; it is composed of coarse-grained fassaite, melilite, spinel, and very fine-grained anorthite groundmass with abundant anhedral inclusions of fassaite. The right portion is mineralogically similar to Type B CAIs and consists of massive melilite intergrown with fassaite and spinel; it also includes a spinel palisade body. The CAI periphery has secondary nepheline and sodalite, and is crosscut by andradite-bearing veins (two veins are labeled by white-red lines in a and c). The core is fractured; the fractures are partly filled by andradite and wollastonite. The inclusion is surrounded by the Wark-Lovering rim sequence of spinel, Al,Ti-diopside, and olivine. andr, andradite; ol, olivine; sod, sodalite; wol, wollastonite.

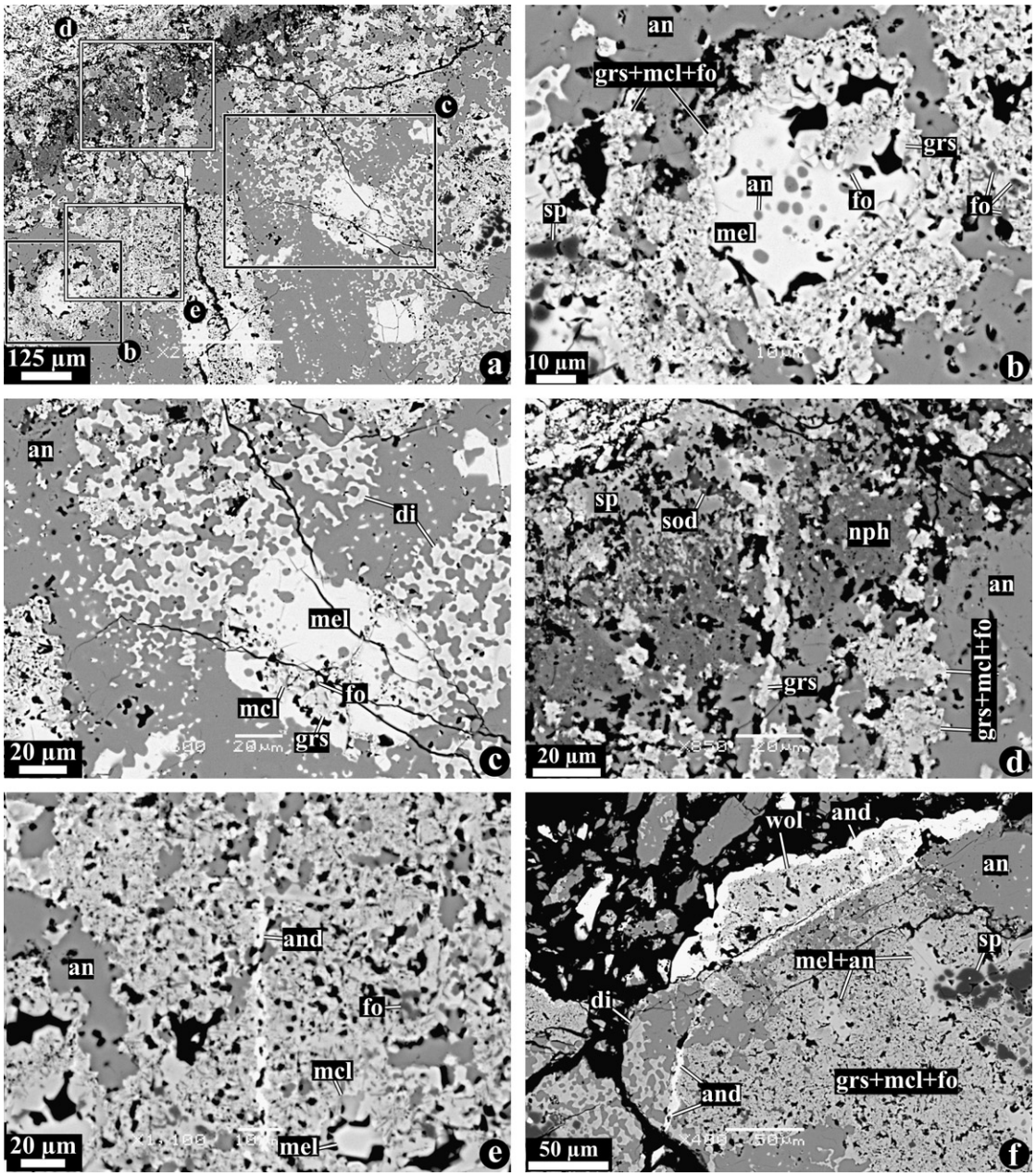

Fig. 7. BSE images of the CAI *6-1-72*. Regions outlined and labelled in (a) are shown in detail in (b–e). Lacy melilite grains are extensively replaced by a fine-grained, porous mixture of grossular, monticellite, and forsterite. Coarse Al,Ti-diopside grains contain abundant inclusions of anorthite. Groundmass anorthite is very fine-grained and contains abundant intergranular, anhedral Al,Ti-diopside. grains The outer portion of the CAI is extensively replaced by nepheline, sodalite, and ferrous olivine; this alteration zone, as well as pyroxene grains, melilite pseudomorphs, and groundmass anorthite are crosscut by the andradite and grossular-bearing veins (a). Andradite coexisting with wollastonite occurs also in fractures in the CAI core (f).

the chondrule consists of Al-bearing (up to 3.5 wt% Al_2O_3) low-Ca pyroxene, olivine (Fa_5), and abundant opaque nodules of sulfides and magnetite (alteration product of Fe,Ni-metal).

Chondrule *3555B-2* (Fig. 14) has an Al-rich core and a ferromagnesian mantle. The core consists of anorthitic plagioclase (An_{90}), partially replaced by nepheline, and interstitial Al-bearing low-Ca pyroxene, (Table 2). The mantle zone consists of polysynthetically twinned low-Ca pyroxene, poikilitically enclosing olivine (Fa_9), and abundant opaque nodules completely replaced by ferrous olivine and Fe,Ni-sulfides.

4. DISCUSSION

4.1. Crystallization sequence of Type C CAIs

Bulk chemical compositions of the Allende Type C CAIs and Al-rich chondrules described here are reported

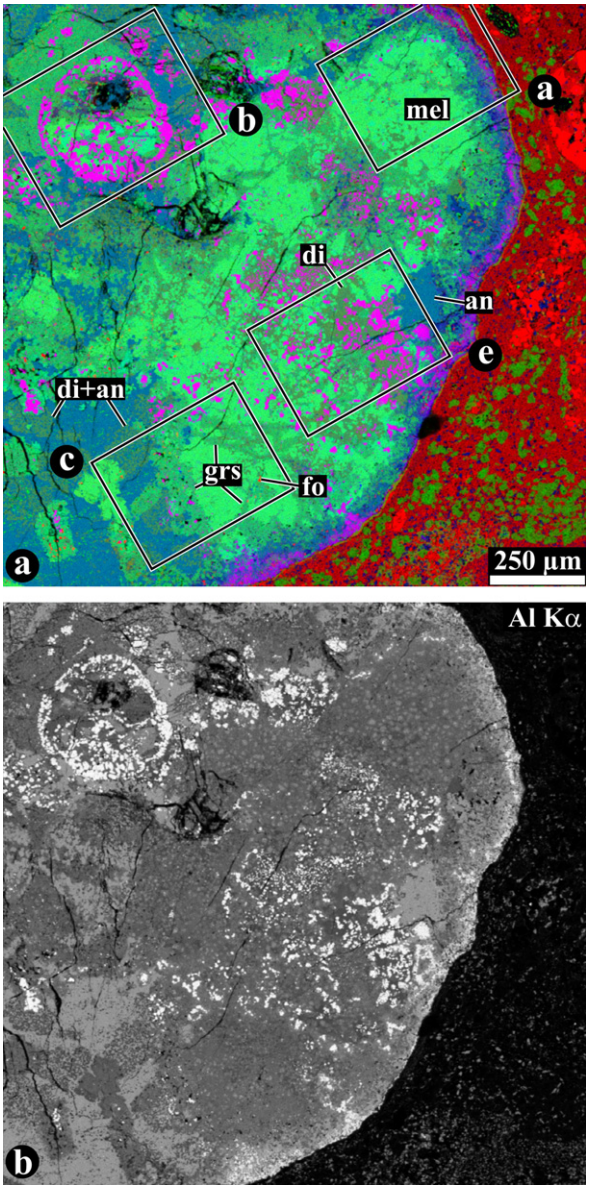

Fig. 8. Combined elemental map in Mg (red), Ca (green), and Al Kα (blue) X-rays (a) and elemental map in Al Kα (b) of the Type B-like portion of the CAI *6-1-72*. Regions outlined and labeled in (a) are shown in detail in Fig. 9.

in Table 2 of Wark (1987). Since the CAI compositions are spinel-saturated, they can be projected from spinel on the gehlenite–anorthite–forsterite plane (Fig. 1AE) and their crystallization sequence can be inferred: sp → sp+an → sp+an+mel (*100*, *160*, *3529-40*, *6-1-72*) or sp+an+di (*TS26*, *ABC*) → sp+an+mel+di. The early crystallization of spinel from Type C CAI-like melts is supported by the experiments of Stolper and Paque (1986) and is consistent with our petrographic observations described above. At the same time, the presence of anorthite-free compact regions of melilite and fassaite overgrown by the same minerals with abundant anorthite inclusions (lacy melilite and fassaite) in the CAIs *100*, *160*, and *6-1-72* (Figs. 5a, 8, 9, and 11e,f) is difficult to reconcile with equilibrium crystallization from Type C CAI melts: precipitation of melilite and fassaite must have preceded crystallization of anorthite, if all these minerals crystallized from the same melt. Wark (1987) suggested that crystallization of anorthite was delayed due to nucleation difficulties and that after the initial, relatively slow stages of Type C CAI melt crystallization, the residual melt was suddenly quenched. This interpretation may explain the lacy textures of melilite and fassaite grains and the very fine-grained groundmass anorthite. We note, however, that no difficulties in nucleation of anorthite are observed in several other Type C CAIs, such as *CG-5*, *ABC*, *TS26*, or *93*, or in experiments on crystallization of Type C CAI-like melts (Paque and Stolper, 1984). We suggest instead that the massive melilite and fassaite in Type C CAIs are relict, which is consistent with systematic differences in chemical compositions of melilite in the Type B and Type C portions of *6-1-72*; the former has lower Na and Åk contents than the latter (Table 2 and Fig. 3).

The predicted crystallization sequence is also inconsistent with the presence of coarse Al,Ti-diopside and melilite grains with abundant anorthite inclusions (lacy textures); the true eutectic intergrowths of melilite, anorthite, and diopside, as observed in the chondrule-bearing Type C CAIs *ABC*, *TS26*, and *93* (Figs. 2a,b, 6, and 10d–f in Krot et al., 2007a) are not observed. Finally, the very fine-grained nature of anorthite in CAIs *100*, *160*, *3529-40*, and *6-1-72* is very different from the typical appearance of igneous anorthite in Type B CAIs from CV chondrites (e.g., Hutcheon et al., 1978; MacPherson et al., 1988; MacPherson, 2003; Fagan et al., 2004). Based on these observations, we infer that the lacy textures of melilite and Al,Ti-diopside and the very fine-grained anorthite in CAIs *100*, *160*, *3529-40*, and *6-1-72* cannot be explained by single stage crystallization from Type C CAI melts; these features may have resulted from remelting of the initially coarse-grained, Type B-like inclusions.

4.2. Origin of primary minerals in the Allende Type C CAIs

Bulk chemical compositions of igneous CAIs are commonly explained as being the result of melting of condensate precursors assembled and melted at different ambient temperatures; the melting was accompanied by evaporation to varying degrees (e.g., Grossman et al., 2000, 2002; Richter et al., 2002). These models satisfactorily explain the bulk chemical compositions of some compact Type A and Type B CAIs, but fail to reproduce those of Type C inclusions, which are anorthite-enriched and forsterite-deficient relative to bulk chemical compositions of condensates from a cooling nebular gas (MacPherson et al., 2004), and show no clear evidence for evaporation from melt: they have high Si/Mg ratios and show enrichments in light Mg isotopes (Wark, 1987).

Wark (1987) suggested that Type C CAIs crystallized from melts condensed from a gas of solar composition at high total pressure and high dust/gas ratio. However, this

hypothesis is inconsistent with thermodynamic model calculations of gas–liquid condensation in dust-rich nebular regions (Yoneda and Grossman, 1995; Ebel and Grossman, 2000), which failed to produce these compositions. In addition, gas–liquid condensation hypothesis is inconsistent with the presence of relict grains in some of the Allende Type C CAIs (Krot et al., 2005b, 2007a, this study).

Beckett and Grossman (1988) suggested that Type C CAIs formed by melting, with little or no volatilization of spinel-rich Type A CAIs, which experienced partial replacement of melilite and spinel by diopside and anorthite:

$$(Ca_2MgSi_2O_7 + Ca_2Al_2SiO_7)_{(mel\ ss)} + MgAl_2O_{4(s)} + 5SiO_{(g)} + 5H_2O_{(g)} = 2CaMgSi_2O_{6(s)} + 2CaAl_2Si_2O_{8(s)} + 5H_{2(g)} \quad (1)$$

$$(Ca_2MgSi_2O_7 + Ca_2Al_2SiO_7)_{mel\ ss} + 5SiO_{(g)} + 2Mg_{(g)} + 7H_2O_{(g)} = 3CaMgSi_2O_{6(s)} + CaAl_2Si_2O_{8(s)} + 7H_{2(g)} \quad (2)$$

The apparently unmelted spinel-anorthite-rich CAIs described in Ningqiang by Lin and Kimura (1998) and in the reduced CV chondrites Efremovka and Leoville by Krot et al. (2004b) and Aléon et al. (2005) may represent such precursor inclusions. These CAIs show clear evidence for replacement, to varying degrees, of melilite and spinel by anorthite and Al-diopside in the CAI-forming region characterized by ^{16}O-rich compositions (Krot et al., 2005a). The concept of fine-grained, spinel-, melilite-rich CAI-like precursors for Type C CAIs is also consistent with Group II rare earth element patterns and enrichment in light Mg isotopes in some of them (Wark, 1987).

The anorthite-enriched and forsterite-deficient bulk compositions of Type C CAIs may be explained by the chemical and physical processes experienced by their precursors. For example, the equilibrium condensation calculations reported by MacPherson et al. (2004) and Petaev and Wood (2005) showed that condensation of anorthite precedes that of forsterite at total pressures $<10^{-4}$ bar; at total pressures $\leqslant 10^{-5}$ bar, the bulk chemical composition of condensates passes through the field of Type C CAIs. Remelting of these precursors prior to condensation of forsterite could have resulted in formation of Type C CAIs. Alternatively, the precursors escaped mixing with forsterite condensates prior to Type C CAI melting event(s) (e.g., if these precursors had rounded, smooth surfaces, without large depressions). We note, however, that some observations (listed below) are difficult to reconcile with the "simple" formation history proposed by Beckett and Grossman (1988), Lin and Kimura (1998), and Krot et al. (2004b); these are listed below.

(i) CAI *6-1-72* contains a relict region texturally and mineralogically similar to Type B CAIs. In addition, CAIs *160* and *100* contain massive melilite and fassaite grains, which are texturally similar to those in the Type B portion of *6-1-72*. These observations suggest that these CAIs formed by melting of coarse-grained, igneous inclusions, not fine-grained nebular condensates. Since bulk compositions of Types B and C CAIs plot in the liquidus fields of melilite and anorthite, respectively, we infer that either the Type B CAI-like precursors had experienced very extensive postcrystallization alteration resulting in addition of Si and formation of anorthite+diopside and/or nepheline+sodalite[1] (alteration and melting processes could have occurred several times) or addition of Si occurred during remelting of Type B-like CAIs, as a result of gas–melt interaction as was proposed for chondrules (Tissandier et al., 2002; Krot et al., 2004d; Libourel et al., 2006).

Although fine-grained, spinel-rich CAI compositions overlap with those of Type Cs (Lin and Kimura, 1998), coarse-grained Type B CAIs with sufficient secondary anorthite and diopside to move their bulk compositions to the field occupied by Type C CAIs have not been observed, suggesting that this may be a rather inefficient process.

Although remelting of Type B CAIs containing nepheline and sodalite appears to be consistent with (1) the high abundance of Na in melilite of Type C CAIs (Fig. 3), (2) the experimentally determined partitioning of Na between melilite and liquid (Beckett et al., 2000), and (3) the inferred evolution of Type B CAIs by multiple stages of alteration and melting (MacPherson and Davis, 1993; Fagan et al., 2006), the nebular origin of nepheline and sodalite remains controversial (e.g., MacPherson et al., 1988; Krot et al., 1998, 2006b and references therein). In addition, a high abundance of Na in melilite of Type C CAIs is also observed in CR chondrites showing no evidence for alkali metasomatic alteration (Aléon et al., 2002; Krot et al., 2005a). Based on these arguments, we infer that addition of Si and Na possibly through gas–melt interaction may be a viable mechanism (see below).

(ii) Most Type B CAIs from CV chondrites show mineralogical and isotopic (mass-dependent fractionation) evidence for volatilization of common elements (e.g., Mg and Si) during crystallization (e.g., Grossman et al., 2002; Davis et al., 2005 and references therein). In contrast, Type C CAIs, which have higher volatile element contents than most Type B CAIs,[2] show no clear evidence for volatilization (Wark, 1987). These observations may indicate that melting of Type C CAIs occurred under high total pressures or high dust/gas ratios, which either stabilized melts and prevented extensive evaporation, or the vaporized elements efficiently recondensed into the CAI melts. Similar conditions have been inferred for chondrule-forming regions (Alexander and Wang, 2000; Alexander et al., 2000; Galy et al., 2000; Desch and Connolly, 2002; Hewins et al., 2005; MacPherson et al., 2005; Cuzzi and Alexander, 2006). This is consistent with the observations that several Type C CAIs from Allende and CR chondrites experienced melting in chondrule-forming regions (Krot et al., 2005a,b, 2007a).

[1] Replacement of melilite by nepheline can be expressed as $Ca_2Al_2SiO_{7(s)} + 2Na_{(g)} + SiO_{(g)} + 2H_2O_{(g)} = 2NaAlSiO_{4(s)} + 2CaO_{(g)} + 2H_{2(g)}$

[2] Some Type B CAIs contain abundant forsterite and may have similar volatility to Type C CAIs. These CAIs, however, show clear evidence for extensive evaporation accompanied by mass-dependent fractionation of O, Mg, and Si isotopes (e.g., Clayton et al., 1984; Davis et al., 1991).

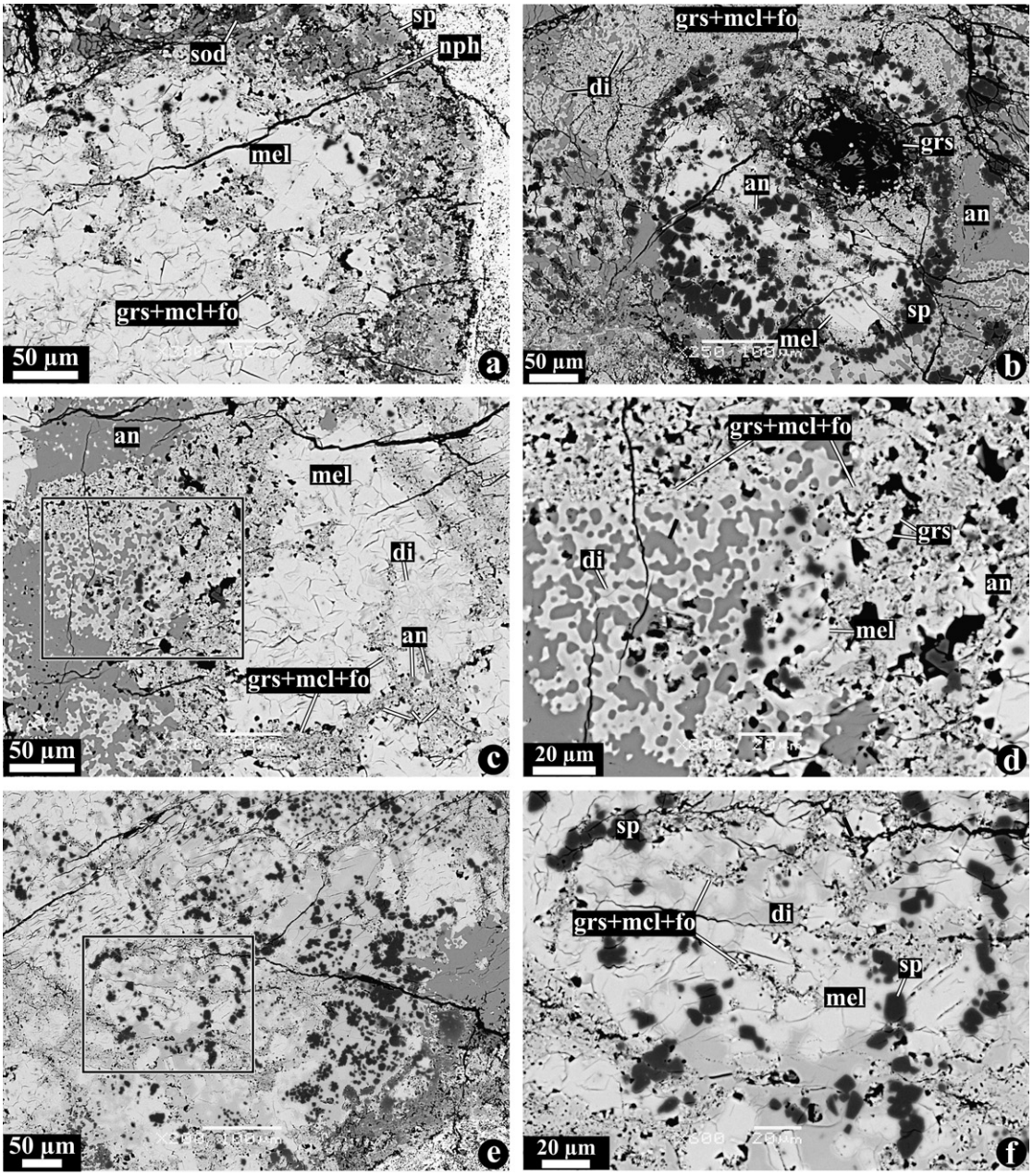

Fig. 9. BSE images of the Type B-like portion of the CAI *6-1-72* (for locations see Figs. 6 and 8). It is largely composed of massive polycrystalline melilite, spinel, and massive and intergranular fassaite. Massive melilite occurs also within a palisade body. Melilite is crosscut by veins of fine-grained grossular, monticellite, and rare forsterite. Both massive melilite and spinel palisade are overgrown by fassaite with abundant inclusions of anorthite and melilite pseudomorphed by a porous mixture of grossular, monticellite, and forsterite.

We infer that at least some Type C CAIs in Allende formed by melting of coarse-grained Type B-like inclusions under conditions where CAI melts were stable, and SiO and Na condensed into these melts. Fig. 15 illustrates the results of gas–melt interaction of a Type B CAI-like melt with $SiO + CO$ gas at 1328 °C and 10^{-2} bar total pressure; the duration of the experiment was 2.5 min. The analytical technique and experimental conditions are discussed in detail by Tissandier et al. (2002). The interaction results in the formation of prismatic anorthite crystals in the peripheral portion of the experimental charge; a very similar texture is observed in a chondrule-bearing Type C CAI *93* (Figs. 9 and 10a–c in Krot et al., 2007a; Fig. 6EA). At this temperature, the melt composition moves from the melilite liquidus field to the liquidus field of anorthite. Interaction at higher temperature (>1370 °C) would result in addition of Si to the melt which will crystallize anorthite under cooling (Fig. 15c). It may explain evolution of Type B CAI-like melts towards Type C inclusions.

We note that similar conditions existed during formation of magnesian chondrules, in which compositions were controlled by gas–melt interaction, not by crystallization of olivine or pyroxene (Libourel et al., 2002, 2006). If correct, chondrules and some igneous CAIs experienced melting

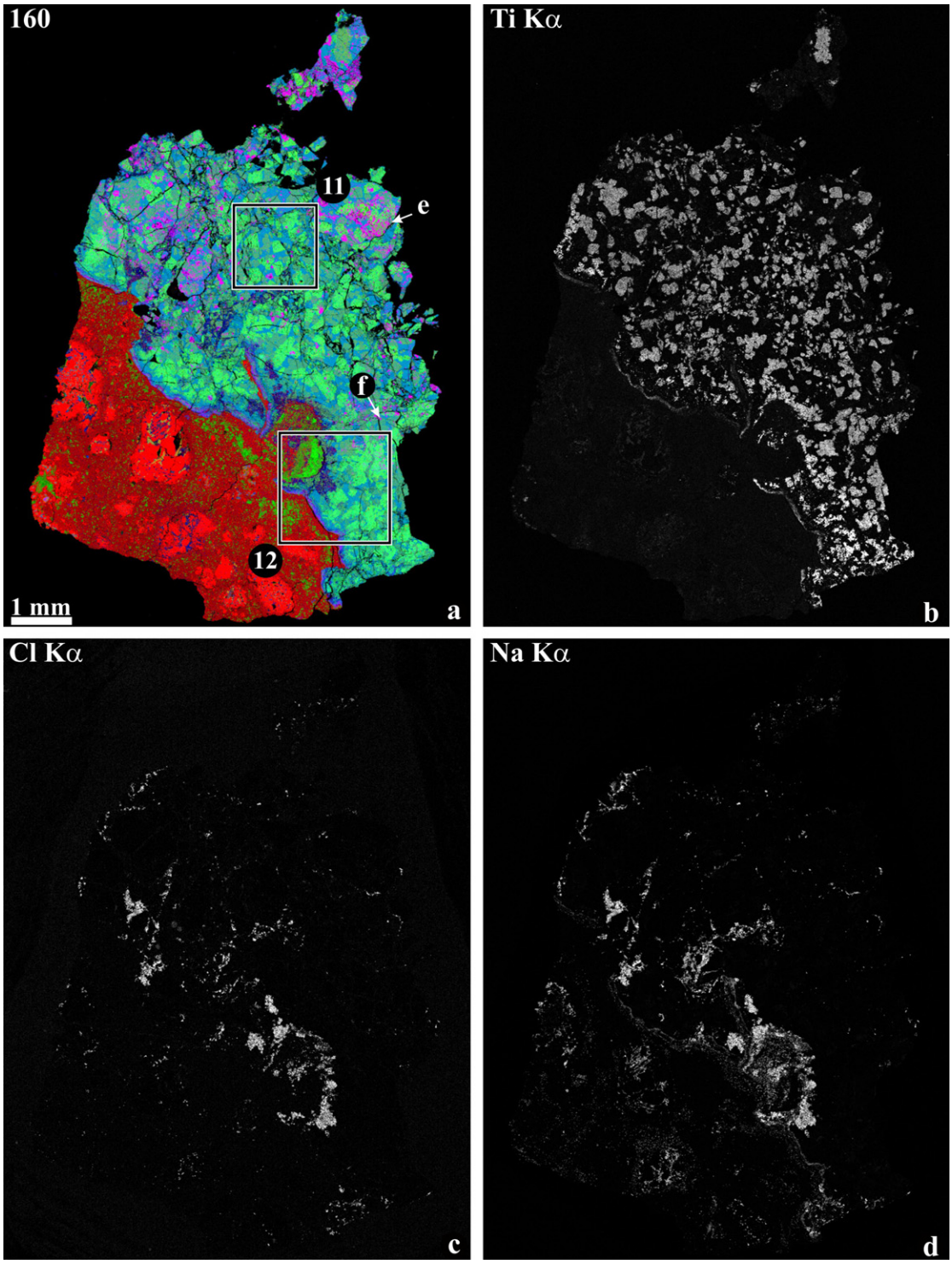

Fig. 10. Combined elemental map in Mg (red), Ca (green), and Al Kα (blue) X-rays (a), and elemental maps in Ti (b), Cl (c) and Na Kα (d) X-rays of a Type C CAI *160*. Regions outlined and labelled in (a) are shown in detail in Figs. 11 and 12; arrows labeled as "e" and "f" indicate regions shown in Fig. 11e and 11f, respectively. The CAI consists of coarse-grained fassaite, melilite, spinel, and groundmass anorthite with abundant anhedral inclusions of fassaite. The CAI is partially surrounded by the Wark-Lovering rim sequence of spinel, Al,Ti-diopside, and olivine, fine-grained accretionary rim, and matrix. One of the depressions on the CAI surface is filled by andradite and wollastonite (green region in left corner of the region labeled as "12"). The outer portion of the CAI is replaced by nepheline and sodalite.

under similar conditions, though not necessarily at the same time in the same nebular region. It remains unclear to what degree bulk compositions of igneous CAIs were defined by their precursor materials, evaporation from melt, or gas–

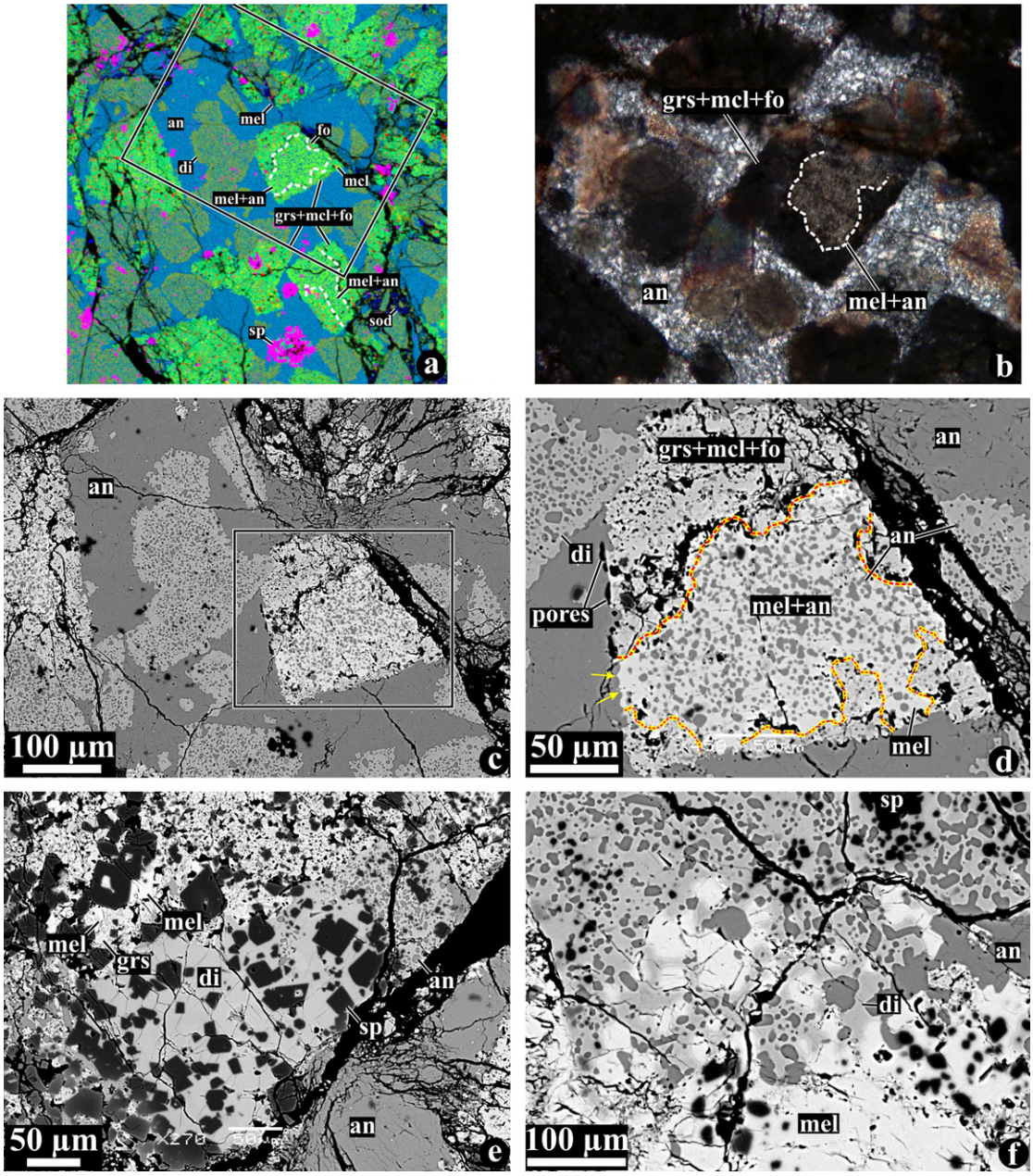

Fig. 11. Combined elemental map in Mg (red), Ca (green), and Al Kα (blue) X-rays (a), optical micrograph in transmitted light (b), and BSE images (c–f) of a central region of the Type C CAI *160* (for location see Fig. 10). Regions outlined in (a) and (c) are shown in detail in (b) and (d), respectively. This region contains lacy melilite and fassaite grains and fine-grained groundmass anorthite. The lacy melilite grains are replaced by a fine-grained, porous mixture of grossular, monticellite, and forsterite. Pores are also observed along the boundaries between the pseudomorphed melilite regions and groundmass anorthite; contacts between relict melilite and groundmass anorthite (indicated by yellow arrows in d) lack pores. (e) Region of massive fassaite with euhedral spinel inclusions, which is overgrown lacy fassaite. (f) Polycrystalline melilite overgrown by lacy fassaite.

melt condensation. It can be potentially estimated from their bulk isotopic compositions.

4.3. Origin of secondary minerals in the Allende Type C CAIs

While Type C CAIs in CR, CO, CH and ungrouped carbonaceous chondrites Adelaide and Acfer 094 are mineralogically pristine (Krot et al., 2001, 2004a, 2006a; Aléon et al., 2002; Itoh et al., 2004), the Allende Type C CAIs typically contain secondary grossular, monticellite, forsterite, wollastonite, sodalite, nepheline, hedenbergite, and andradite. Secondary grossular is a ubiquitous phase in the Allende Type B CAIs as well, where it forms veins in melilite, euhedral crystals lining cavities in melilite and anorthite, and is predominantly intergrown with monticellite at melilite–anorthite contacts; occasionally, grossular

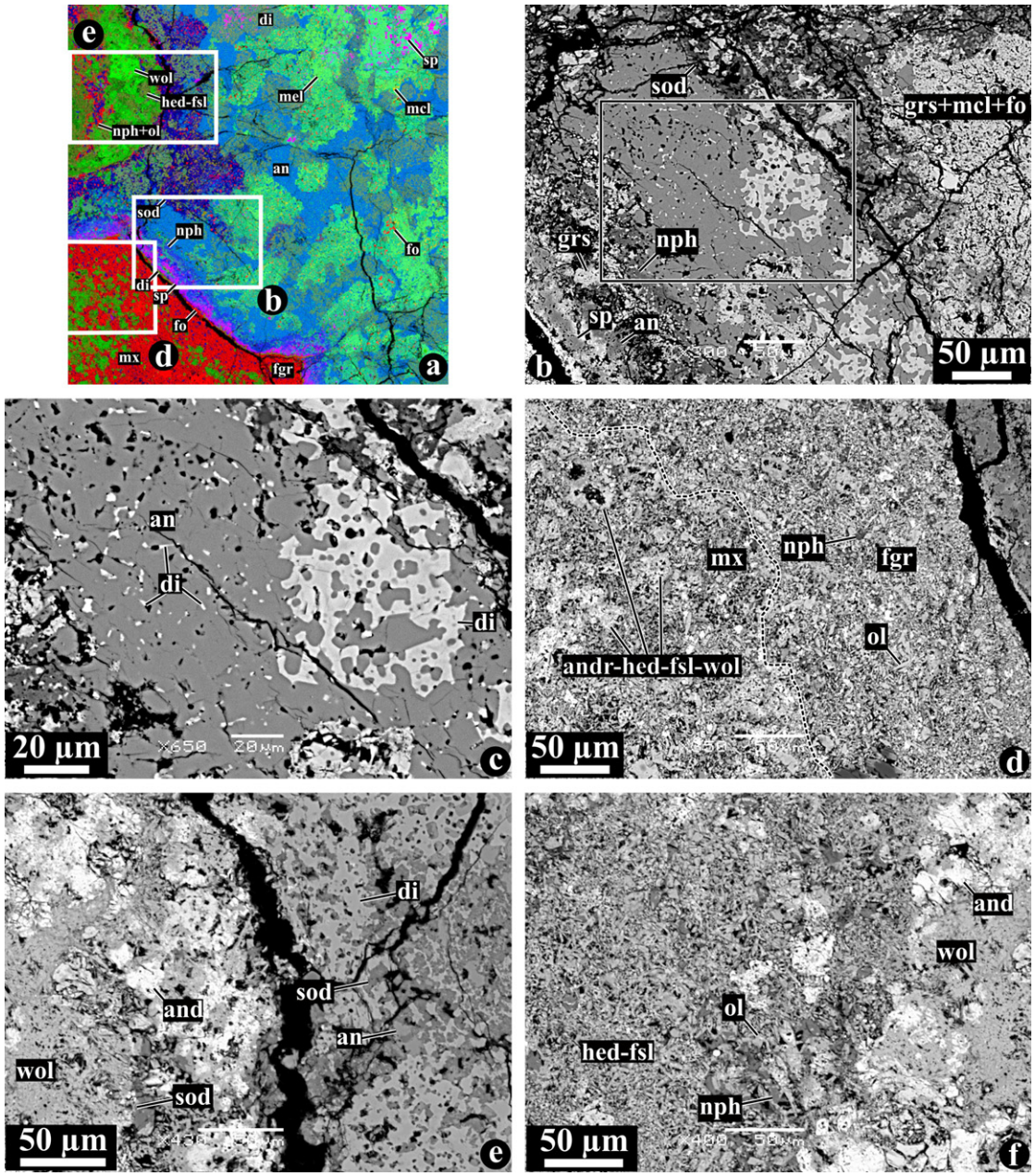

Fig. 12. Combined elemental map in Mg (red), Ca (green), and Al Kα (blue) X-rays (a) and BSE images (b–f) of a peripheral region of the Type C CAI *160* (for location see Fig. 10). Regions outlined in (a) and (b) are shown in detail in (b–e). This region contains nearly complete pseudomorphs after melilite, lacy fassaite, and fine-grained anorthite groundmass with abundant intergranular inclusions of fassaite. Anorthite in the CAI mantle is replaced by sodalite and nepheline. (d) The Wark-Lovering layers of spinel, Al,Ti-diopside, and olivine are surrounded by a fine-grained accretionary rim (fgr) largely composed of ferrous olivine, and matrix containing abundant nodules of andradite–hedenbergite–wollastonite. (e and f) A depression on the surface of the CAIs is filled by andradite and wollastonite.

is associated with wollastonite (e.g., Hutcheon et al., 1978; Hutcheon and Newton, 1981; Fagan et al., 2006). Based on these observations, Hutcheon and Newton (1981) suggested that grossular and monticellite formed via the closed-system reaction:

$$3Ca_2MgSi_2O_7 + Ca_2Al_2SiO_7 + CaAl_2Si_2O_8 = 2Ca_3Al_2Si_3O_{12} + 3CaMgSiO_4. \quad (3)$$

From the measured melilite composition ($Åk_{52}$) at the grossular–monticellite margin, they estimated an apparent equilibrium temperature for the formation of grossular of 668 °C and concluded that this reaction occurred in the solar nebula during a prolonged heating event. Based on the apparent rarity of monticellite associated with grossular and the common occurrences of spinel in Type C CAIs in Allende, Wark (1987) proposed

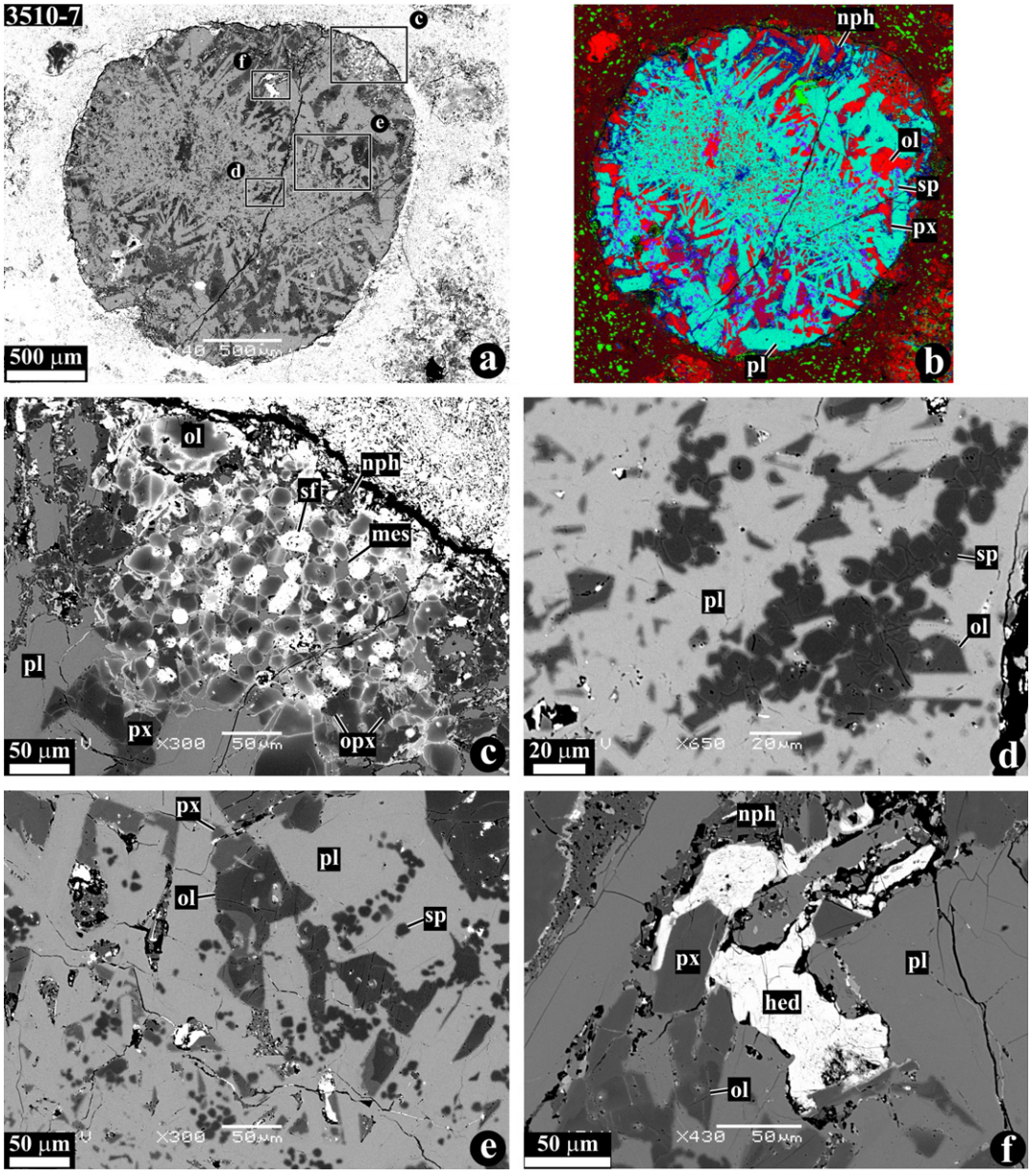

Fig. 13. BSE images (a and c–f) and combined elemental map in Mg (red), Ca (green), and Al Kα (blue) X-rays (b) of an Al-rich chondrule *3510-7*. Regions outlined in (a) are shown in detail in (c–f). Region shown in (c) is composed of olivine (ol), low-Ca pyroxene (opx), and abundant sulfide (sf) nodules; it is texturally and mineralogically similar to Type I chondrules. The rest of the chondrule is almost free of opaque nodules and consists of lath-shaped anorthitic plagioclase (pl), forsteritic olivine, fine-grained spinel, and Al-bearing low-Ca pyroxene. Plagioclase and possibly mesostasis in the outer part of the chondrule are replaced by nepheline; hedenbergite occupies interstitial regions between plagioclase laths.

another reaction to form grossular, which can proceed below 724 °C:

$$2Ca_2Al_2SiO_7 + CaAl_2Si_2O_8 + CaMgSi_2O_6 = 2Ca_3Al_2Si_3O_{12} + MgAl_2O_4. \quad (4)$$

However, no textural observations were described to support this reaction; this mechanism is also inconsistent with our petrographic observations described above, which indicate that spinel is a primary igneous mineral, not a by-product of alteration of melilite.

In CAIs *100*, *160*, *3529-40* and *6-1-72*, lacy melilite grains are pseudomorphed by grossular, monticellite, ±forsterite, suggesting that in addition to reaction (1), another closed-system, isochemical reaction took place:

$$3Ca_2MgSi_2O_7 + Ca_2Al_2SiO_7 + 2CaAl_2Si_2O_8 = 3Ca_3Al_2Si_3O_{12} + CaMgSiO_4 + Mg_2SiO_4. \quad (5)$$

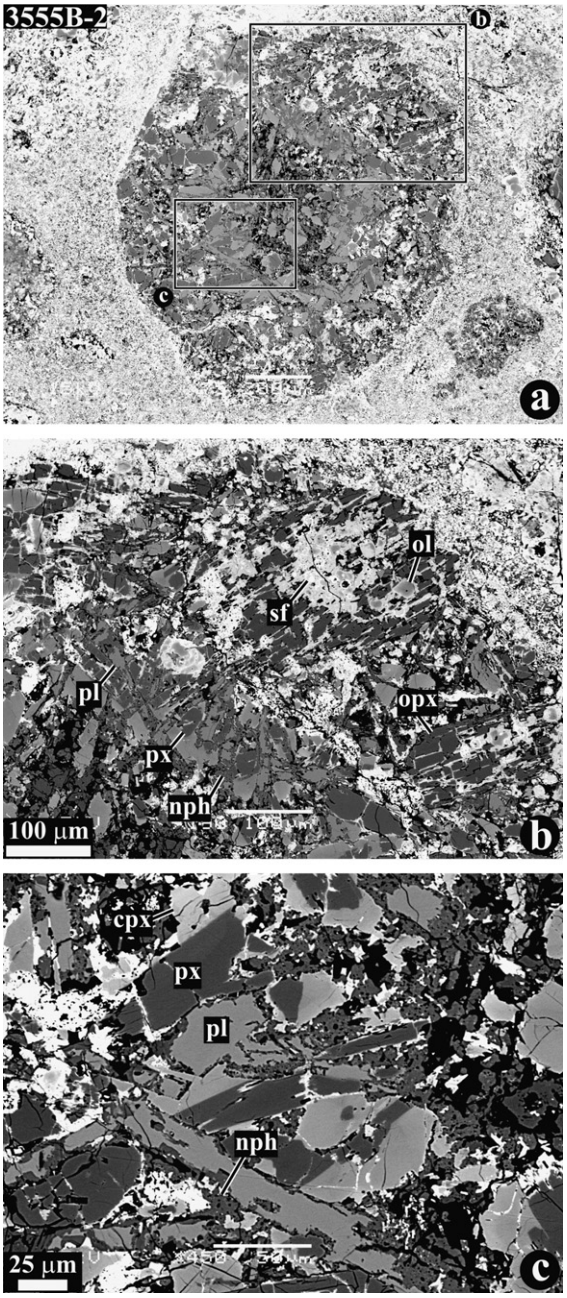

Fig. 14. BSE images of an Al-rich chondrule *3555B-2*. Regions outlined in (a) are shown in detail in (b) and (c). The chondrule core consists of lath-shaped anorthitic plagioclase (pl) corroded by nepheline (nph), Al-bearing low-Ca pyroxene (px) and high-Ca pyroxene (cpx). Its mantle zone is composed of low-Ca pyroxene (opx) poikilitically enclosing olivine (ol) and opaque nodules extensively replaced by ferrous olivine and Ni-bearing sulfides (sf).

Although under equilibrium conditions for melilite of $Åk_{\sim 30-60}$ (typical range of melilite compositions of Type C CAIs) this reaction occurs below 760 °C (Fig. 16), the common presence of unaltered melilite–anorthite intergrowths in the Allende Type C CAIs suggests the lack of equilibrium (e.g., Figs. 5b–f, 7a–c, and 11a–d). As a result, this reaction can only be used to constrain the upper temperature of grossular formation.

Gehlenitic melilite in the Type B portion of *6-1-72* has been largely replaced by grossular and monticellite; however, forsterite is very minor (Figs. 8 and 9). There is no clear evidence that anorthite participated in this reaction (i.e., reaction (2) is not applicable). These observations may indicate an open-system alteration of melilite:

$$Ca_2MgSi_2O_7 + Ca_2Al_2SiO_7 + SiO_2 = Ca_3Al_2Si_3O_{12} + CaMgSiO_4. \quad (6)$$

The chondrule-bearing Type C CAIs *ABC*, *TS26*, and *93* contain secondary grossular, monticellite, and wollastonite replacing melilite and anorthite-rich mesostasis (see Figs. 2a–e, 6, and 10e–f in Krot et al., 2007a; Fig. 7EA), suggesting the following isochemical reaction:

$$4Ca_2MgSi_2O_7 + Ca_2Al_2SiO_7 + CaAl_2Si_2O_8 = 2Ca_3Al_2Si_3O_{12} + 4CaMgSiO_4 + CaSiO_3. \quad (7)$$

Although both nebular and asteroidal heating could have resulted in formation of grossular in the Allende Type C CAIs, the former appears to be less attractive for several reasons. (i) Aluminum–magnesium systematics of most grossular grains analyzed so far (MacPherson, 2003 and references therein) suggest its very late-stage formation, which is difficult to reconcile with prolonged nebular heating (Hutcheon and Newton, 1981). We note, however, that a high initial $^{26}Al/^{27}Al$ ratio $\sim 3 \times 10^{-5}$ has been recently inferred for one of the grossular grains from the Allende Type B2 CAI; secondary grossular and sodalite in the same CAIs show small $^{26}Mg^*$ corresponing to the initial $^{26}Al/^{27}Al$ ratio of $(4.7 \pm 2.6) \times 10^{-6}$ (Fagan et al., 2006). If these observed excesses in ^{26}Mg of the Allende grossular and sodalite are not inherited from the replaced melilite and anorthite, multistage formation of grossular would be required. At the same time, there is no disagreement that Allende experienced prolonged thermal metamorphism in an asteroidal setting at $\geqslant 350$ °C (e.g., Bonal et al., 2006 and references therein). (ii) Secondary grossular occurs also in the Allende chondrules, suggesting that both CAIs and chondrules experienced similar thermal processing (Krot et al., 1998 and references therein). (iii) Neither CAIs nor chondrules in the reduced CV chondrites show evidence for secondary grossular; it is also absent in aqueously altered oxidized chondrites of the Bali-like subgroup, which experienced lower temperature thermal metamorphism than Allende (Bonal et al., 2006).

Anorthite in outer portions of the Allende Type C CAIs is replaced by nepheline and sodalite; spinel in these altered regions is enriched in FeO. These observations suggest that the CAIs experienced open-system iron–alkali metasomatic alteration with Na, Cl, and Fe being introduced and Ca preferentially lost. This alteration may have either postdated formation of grossular–monticellite–forsterite pseudomorphs or both processes took place contemporaneously. We note that the presence of abundant hedenbergite–wollastonite–andradite nodules in the oxidized CV matrices could be a by-product of this type of alteration (Krot et al., 1998). The alkali-rich peripheries of the CAIs and pseudomorphed melilite grains are crosscut by andradite-bearing veins, indicating that they postdate both secondary mineral assemblages.

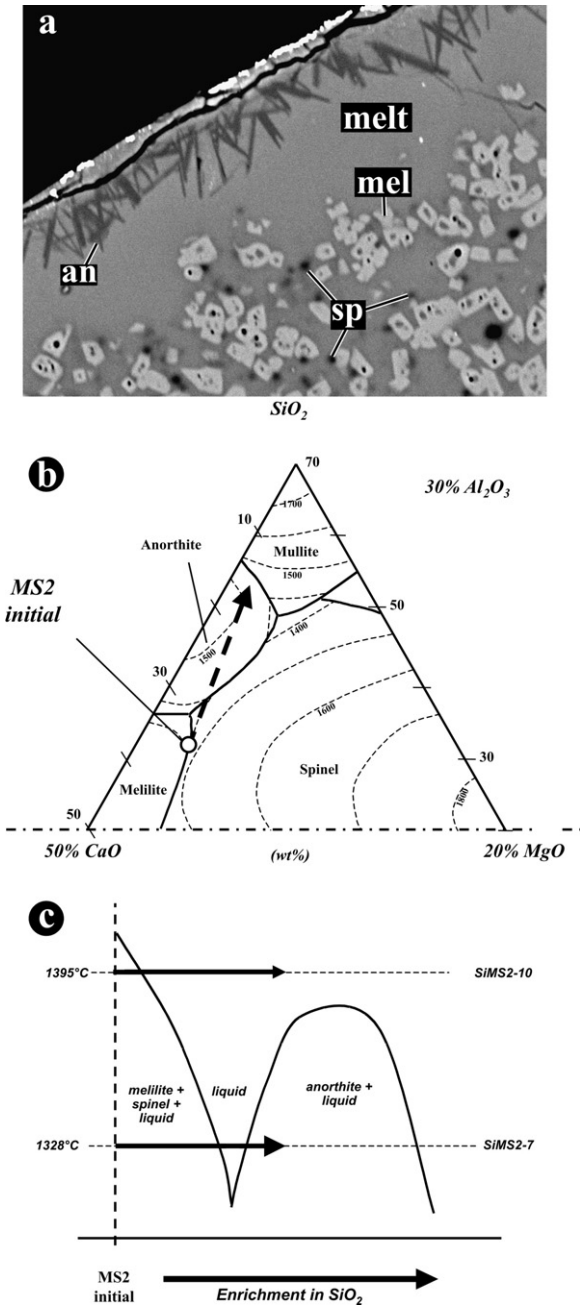

Fig. 15. (a) BSE image of experimental charge of a Type B CAI-like bulk composition (in wt%: MgO, 5.3, SiO_2, 29.9, Al_2O_3, 32.5, and CaO, 32.3) that was exposed at 1328 °C to SiO + CO gas for 2.5 min. an, anorthite; mel, melilite; sp, spinel. (b) Gas–melt interaction resulted in evolution of melt composition from melilite liquidus field to anorthite liquidus field and nucleation of prismatic anorthite crystals in the peripheral zone of the charge. (c) Isothermal interaction of the melt at higher temperature would result in increase of its Si content without nucleation of anorthite.

We infer that secondary grossular, forsterite, monticellite, nepheline, sodalite, ferrous olivine, hedenbergite, and andradite in the Allende Type C CAIs most likely formed during asteroidal thermal processing.

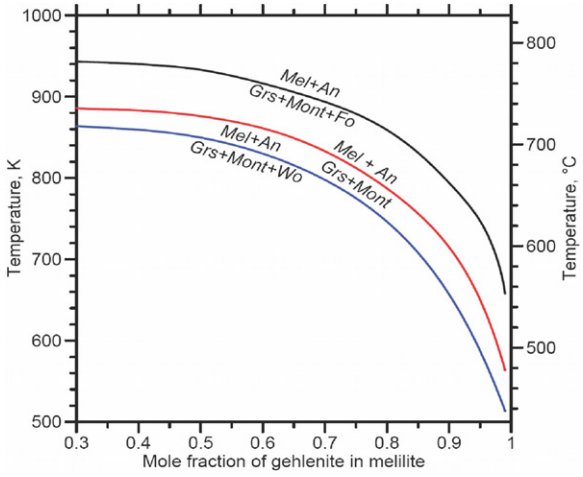

Fig. 16. Equilibrium calculations illustrating equilibrium temperature for the formation of grossular, monticellite, and forsterite or wollastonite by replacement of melilite and anorthite. Lack of equilibrium in the Allende Type C CAIs does not allow estimating of the formation temperature of grossular-bearing assemblages.

5. CONCLUSIONS

[1.] The coarse-grained, igneous, anorthite-rich (Type C) CAIs from Allende have diverse textures and mineralogies, suggesting complex nebular and asteroidal formation histories. Three of these CAIs (*ABC*, *TS26*, and *93*) with very sodium-rich åkermanitic melilite ($Åk_{63–74}$, 0.4-0.6 wt% Na_2O) and Cr-bearing Al,Ti-diopside contain chondrule-like materials (forsteritic olivine, low-Ca pyroxene, and high-Ca pyroxene) in their peripheral portions. The CAIs *100*, *160*, *6-1-72*, and *3529-40* contain relict coarse-grained regions, which are texturally and mineralogically similar to the Allende Type B CAIs and are overgrown by fassaite and Na-bearing åkermanitic melilite ($Åk_{30–75}$, 0.1–0.4 wt% Na_2O) grains with abundant rounded inclusions of anorthite, ~5–10 μm in size; all are embedded into a similarly fine-grained anorthite groundmass. The melilite–anorthite grains in these CAIs are pseudomorphed to varying degrees by grossular, monticellite, and pure forsterite (*100*, *160*, *6-1-72*, and *3529-40*) or wollastonite (*ABC*, *TS26*, and *93*). Melilite and anorthite in the CAI peripheries are replaced by nepheline and sodalite, which are crosscut by andradite-bearing veins; spinel is enriched in FeO. The CAI fragment *CG5* is exceptionally rich in spinel poikilitically enclosed by Na-free gehlenitic melilite ($Åk_{20–30}$), fassaite, and lath-shaped anorthite; none of the minerals show evidence for alteration.

[2.] The Al-rich chondrules *3655b-2* and *3510-7* contain the Al-rich and ferromagnesian portions; the former are made of anorthitic plagioclase, Al-rich low-Ca pyroxene, and Cr-bearing spinel; the latter consist of fosteritic olivine, low-Ca pyroxene, and opaque nodules.

[3.] We conclude that CAIs *100*, *160*, *6-1-72*, and *3529-40* formed by incomplete melting of coarse-grained Type B-like CAIs, which either experienced extensive

replacement of melilite and spinel by anorthite and diopside (traces of secondary Na-bearing minerals, e.g., nepheline or sodalite, might have formed as well), or silica and sodium were added during melting event.

[4.] *CG5* could have formed by melting of fine-grained CAI with melilite and spinel partially replaced anorthite and diopside.

[5.] CAIs *ABC*, *93*, and *TS-26* experienced melting in the chondrule-forming regions with addition of chondrule-like material, such as forsteritic olivine and low-Ca pyroxene.

[6.] Anorthite-rich chondrules formed by melting of the Al-rich (Type C CAI-like) precursors mixed with ferromagnesian, Type I chondrule-like precursors, supporting the earlier conclusion of Beckett and Grossman (1988).

[7.] The CAIs experienced thermal metamorphism, which resulted in pseudomorphic replacement of melilite and anorthite by grossular, monticellite, and forsterite (*100*, *160*, *6-1-72*, *3592-400*) or by grossular, monticellite, and wollastonite (*ABC*, *93*, *TS-26*). The pseudomorphic replacement was followed or accompanied by iron–alkali metasomatic alteration resulting in replacement of melilite and anorthite by nepheline and sodalite, enrichment of spinel in FeO, and precipitation of salite–hedenbergite pyroxenes, wollastonite, and andradite in fractures and pores in and around CAIs. These alteration processes most likely occurred in an asteroidal setting during prolonged thermal metamorphism, rather than in the solar nebula.

ACKNOWLEDGMENTS

This work was supported by NASA Grants NAG5-10610 (A.N. Krot, P.I.), NAG5-11591 (K. Keil, P.I.), W-19,894 (I.D. Hutcheon, P.I.), NAG5-10468 (G.J. MacPherson, P.I.), and Monkasho grants (H. Yurimoto, P.I.). We thank H. Connolly, R. Hewins, S. Russell and anonymous reviewer for their comments and suggestions which helped to improve the paper. This work was performed under the auspices of the U.S. Department of Energy by the University of California, Lawrence Livermore National Laboratory under Contract No. W-7405-Eng-48.

APPENDIX A. SUPPLEMENTARY DATA

Supplementary data associated with this article can be found, in the online version, at doi:10.1016/j.gca.2007.03.040.

REFERENCES

Aléon J., Krot A. N. and McKeegan K. D. (2002) Ca–Al-rich inclusions and amoeboid olivine aggregates from the CR carbonaceous chondrites. *Meteorit. Planet. Sci.* **37**, 1729–1755.

Aléon J., Krot A. N., McKeegan K. D., MacPherson G. J. and Ulyanov A. A. (2005) Fine-grained, spinel-rich inclusions from the reduced CV chondrite Efremovka: II. Oxygen isotopic compositions. *Meteorit. Planet. Sci.* **40**, 1043–1058.

Alexander C. M. O'D. and Wang J. (2000) Iron isotopes in chondrules: implications for the role of evaporation during chondrule formation. *Meteorit. Planet. Sci.* **36**, 419–428.

Alexander C. M. O'D., Grossman J. N., Wang J., Zanda B., Bourot-Denise M. and Hewins R. H. (2000) The lack of potassium-isotope fractionation in Bishunpur chondrules. *Meteorit. Planet. Sci.* **35**, 859–868.

Beckett J. R. and Grossman L. (1988) The origin of type C inclusions from carbonaceous chondrites. *Earth Planet. Sci. Lett.* **89**, 1–14.

Beckett J. R., Simon S. B. and Stolper E. (2000) The partitioning of Na between melilite and liquid: part II. Applications to type B inclusions from carbonaceous chondrites. *Geochim. Cosmochim. Acta* **64**, 2519–2534.

Bischoff A. and Keil K. (1984) Al-rich objects in ordinary chondrites—related origin of carbonaceous and ordinary chondrites and their constituents. *Geochim. Cosmochim. Acta* **48**, 693–709.

Bonal L., Quirico E., Bourot-Denise M. and Montagnac G. (2006) Determination of the petrologic type of CV3 chondrites by Raman spectroscopy of included organic matter. *Geochim. Cosmochim. Acta* **70**, 1849–1863.

Clayton R. N., MacPherson G. J., Hutcheon I. D., Davis A. M., Grossman L., Mayeda T. K., Molini-Velsko C., Allen J. M. and El Goresy A. (1984) Two forsterite-bearing FUN inclusions in the Allende meteorite. *Geochim. Cosmochim. Acta* **48**, 535–548.

Cuzzi J. N. and Alexander C. M. O'D. (2006) Chondrule formation in particle-rich nebular regions at least hundreds of kilometres across. *Nature* **441**, 483–485.

Davis A. M., MacPherson G. J., Clayton R. N., Mayeda T. K., Sylvester P. J., Grossman L., Hinton R. W. and Laughlin J. R. (1991) Melt solidification and late-stage evaporation in the evolution of a FUN inclusion from the Vigarano C3V chondrite. *Geochim. Cosmochim. Acta* **55**, 621–637.

Davis A. M., Alexander C. M. O'D., Nagahara H. and Richter F. M. (2005) Evaporation and condensation during CAI and chondrule formation. In *Chondrules and the Protoplanetary Disk*, vol. 341 (eds. A. N. Krot , E. R. D. Scott, and B. Reipurth). ASP Conference Series , pp. 433–455.

Desch S. J. and Connolly, Jr., H. C. (2002) A model of the thermal processing of particles in the solar nebula shocks: application to the cooling rates of chondrules. *Meteorit. Planet. Sci.* **37**, 183–207.

Ebel D. S. and Grossman L. (2000) Condensation in dust-enriched systems. *Geochim. Cosmochim. Acta* **64**, 339–366.

Fagan T. J., Krot A. N., Keil K. and Yurimoto H. (2004) Nebular setting of oxygen isotopic alteration in a coarse-grained Ca–Al-rich inclusion from Efremovka. *Meteorit. Planet. Sci.* **39**, 1257–1272.

Fagan T. J., Guan Y. and MacPherson G. J. (2006) Al–Mg isotopic constraints on alteration of Allende Ca–Al-rich inclusions (abstract). *Lunar Planet. Sci.* XXXVII, #1213.

Galy A., Young E. D., Ash R. D. and O'Nions R. K. (2000) The formation of chondrules at high gas pressures in the solar nebula. *Science* **290**, 1751–1753.

Grossman L., Ebel D. S., Simon S. B., Davis A. M., Richter F. M. and Parsad N. M. (2000) Major element chemical and isotopic compositions of refractory inclusions in C3 chondrites: the separate roles of condensation and evaporation. *Geochim. Cosmochim. Acta* **64**, 2879–2894.

Grossman L., Ebel D. S. and Simon S. B. (2002) Formation of refractory inclusions by evaporation of condensate precursors. *Geochim. Cosmochim. Acta* **66**, 145–161.

Hewins R. H., Connolly Jr., H. C. Lofgren G. E. and Libourel G. (2005) Experimental constraints on chondrule formation. In

Chondrites and the Protoplanetary Disk, vol. 341 (eds. A. N. Krot, E. R. D. Scott and B. Reipurth). Astronomical Society of the Pacific Conference Series, p. 286.

Huss G. R., MacPherson G. J., Davis A. M., Krot A. N. and Ulyanov A. A. (2002) Microdistribution of REE in fine-grained group II CAIs in Efremovka (abstract). *Meteorit. Planet. Sci.* **37**, A68.

Hutcheon I. D. and Newton R. C. (1981) Mg isotopes, mineralogy, and mode of formation of secondary phases in C3 refractory inclusions (abstract). *Lunar. Planet. Sci.* **XII**, 491–493.

Hutcheon I. D., Steele I. M., Smith J. V. and Clayton R. N. (1978) Ion microprobe, electron microprobe and cathodoluminescence data for Allende inclusions with emphasis on plagioclase chemistry. *Proc. Lunar Planet. Sci. Conf.* **9**, 1345–1368.

Imai H. and Yurimoto H. (2000) Oxygen and magnesium isotopic distributions in a Type C CAI from the Allende meteorite (abstract). *Lunar Planet. Sci.* **XXXI**, #1510.

Itoh S., Kojima H. and Yurimoto H. (2004) Petrography and oxygen isotopic compositions in refractory inclusions from CO chondrites. *Geochim. Cosmochim. Acta* **68**, 183–194.

Kita N. T., Lin Y., Kimura M. and Morishita, Y. (2004). The ^{26}Al-^{26}Mg chronology of a Type C CAI and POIs in Ningqiang carbonaceous chondrite (abstract). Lunar Planet. Sci. **XXXV**, #1471.

Krot A. N. and Keil K. (2002) Anorthite-rich chondrules in CR and CH carbonaceous chondrites: Genetic link between Ca, Al-rich inclusions and ferromagnesian chondrules. *Meteorit. Planet. Sci.* **37**, 91–111.

Krot A. N., Petaev M. I., Scott E. R. D., Choi B.-G., Zolensky M. E. and Keil K. (1998) Progressive alteration in CV3 chondrites: more evidence for asteroidal alteration. *Meteorit. Planet. Sci.* **33**, 1065–1085.

Krot A. N., Hutcheon I. D. and Huss G. R. (2001) Aluminum-rich chondrules and associated refractory inclusions in the unique carbonaceous chondrite Adelaide (abstract). *Meteorit. Planet. Sci.* **36**(Suppl.), A105–A106.

Krot A. N., Hutcheon I. D. and Keil K. (2002) Anorthite-rich chondrules in the reduced CV chondrites: evidence for complex formation history and genetic links between CAIs and ferromagnesian chondrules. *Meteorit. Planet. Sci.* **37**, 155–182.

Krot A. N., Fagan T. J., Keil K., McKeegan K. D., Sahijpal S., Hutcheon I. D., Petaev M. I. and Yurimoto H. (2004a) Ca,Al-rich inclusions, amoeboid olivine aggregates, and Al-rich chondrules from the unique carbonaceous chondrite Acfer 094: I. Mineralogy and petrology. *Geochim. Cosmochim. Acta* **68**, 2167–2184.

Krot A. N., MacPherson G. J., Ulyanov A. A. and Petaev M. I. (2004b) Fine-grained, spinel-rich inclusions from the reduced CV chondrites Efremovka and Leoville: I. Mineralogy, petrology, and bulk chemistry. *Meteorit. Planet. Sci.* **39**, 1517–1553.

Krot A. N., Yurimoto H., Petaev M. I., Hutcheon I. D. and Wark D. A. (2004c) Type C CAIs: new insights into the early solar system processes (abstract). *Meteorit. Planet. Sci.* **39**(Suppl.), A57.

Krot A. N., Libourel G., Goodrich C. A. and Petaev M. I. (2004d) Silica-rich igneous rims around magnesian chondrules in CR carbonaceous chondrites: evidence for fractional condensation during chondrule formation. *Meteorit. Planet. Sci.* **39**, 1931–1955.

Krot A. N., Hutcheon I. D., Yurimoto H., Cuzzi J. N., McKeegan K. D., Scott E. R. D., Libourel G., Chaussidon M., Aléon J. and Petaev M. I. (2005a) Evolution of oxygen isotopic composition in the inner solar nebula. *Astrophys. J.* **622**, 1333–1342.

Krot A. N., Yurimoto H., Hutcheon I. D. and MacPherson G. J. (2005b) Relative chronology of CAI and chondrule formation: evidence from chondrule-bearing igneous CAIs. *Nature* **434**, 998–1001.

Krot A. N., Ulyanov A. A. and Ivanova M. A. (2006a) Refractory inclusions and aluminum -rich chondrules in the CB/CH- like carbonaceous chondrite Isheyevo. (abstract). *Lunar Planet. Sci.* **XXXVII**, #1226.

Krot A. N., Yurimoto H., Hutcheon I. D., MacPherson G. J. and Paque J. (2007a) Remelting of refractory inclusions in the chondrule-forming regions: evidence from the chondrule-bearing Type C calcium–aluminum-rich inclusions from Allende. *Meteorit. Planet. Sci.* (in press).

Krot A. N., Hutcheon I. D., Brearley A. J., Pravdivtseva O. V., Petaev M. I. and Hohenberg C. M. (2006b) Timescales for secondary alteration of chondritic meteorites. In *Meteorites and The Early Solar System II* (eds. D. Lauretta and H. Y. McSween Jr.), pp. 525–553.

Krot A. N., Chaussidon M., Yurimoto H., Sakamoto N., Nagashima K., Hutcheon I. D. and Hua X. (2007b) Oxygen isotopic compositions of the Allende Type C CAIs: evidence for isotopic exchange during nebular melting and asteroidal thermal metamorphism (abstract). Lunar Planet. Sci. 38, #1918.

Libourel G., Krot A. N., Tissandier L. and Robert F. (2002) Open system behavior of common and moderately volatile elements during chondrule formation (abstract). *Meteorit. Planet. Sci.* **37**(Suppl.), A87.

Libourel G., Krot A. N. and Tissandier L. (2006) Role of gas–melt interaction during chondrule formation. *Earth Planet. Sci. Lett.* **251**, 232–240.

Lin Y. and Kimura M. (1998) Anorthite-spinel-rich inclusions in the Ningqiang carbonaceous chondrite: genetic links to Type A and C inclusions. *Meteorit. Planet. Sci.* **33**, 435–446.

Lin Y. and Kimura M. (2003) Ca–Al-rich inclusions from the Ningqiang meteorite: continuous assemblages of nebular condensates and genetic link to Type B inclusions. *Geochim. Cosmochim. Acta* **67**, 2251–2267.

Lin Y., Kimura M. and Wang D. (2003) Fassaites in compact Type A Ca–Al-rich inclusions in the Ningqiang carbonaceous chondrite: evidence for heating event in the nebula. *Meteorit. Planet. Sci.* **38**, 407–417.

MacDougall J. D., Kerridge J. F. and Phinney D. (1981) Refractory ABC (abstract). *Lunar Planet. Sci.* **XII**, 643–645.

MacPherson G. J. (2003) *Meteorites, Comets and Planets*, vol. 1 (ed. A. M. Davis) *of Treatise on Geochemistry* (eds. H. D. Holland and K. K. Turekian), Elsevier-Pergamon, Oxford, pp. 201–246.

MacPherson G. J. and Davis A. M. (1993) A petrologic and ion microprobe study of a Vigarano Type B2 refractory inclusion: evolution by multiple stages of alteration and melting. *Geochim. Cosmochim. Acta* **57**, 231–243.

MacPherson G. J. and Huss G. R. (2005) Petrogenesis of Al-rich chondrules: evidence from bulk compositions and phase equilibria. *Geochim. Cosmochim. Acta* **69**, 3099–3127.

MacPherson G. J., Wark D. A. and Armstrong J. T. (1988) Primitive material surviving in chondrites—refractory inclusions. In *Meteorites and the Early Solar System* (eds. J. F. Kerridge and M. S. Matthews). University of Arizona Press, Tucson, Arizona, pp. 746–807.

MacPherson G. J., Petaev M. I. and Krot A. N. (2004) Bulk compositions of CAIs and Al-rich chondrules: implications of the reversal of the anorthite/forsterite condensation sequence at low nebular pressures (abstract). *Lunar Planet. Sci.* **XXXV**, #1893.

MacPherson G.J., Simon S. B., Davis A.M., Grossmon L. and Krot A. N. (2005) Calcium–aluminum-rich inclusions: Major unanswered questions. In *Chondrites and the Protoplanetary*

Disk, vol. 341 (eds. A. N. Krot, E. R. D. Scott and B. Reipurth). Astronomical Society of the Pacific Conference Series, pp. 225–250.

Paque J. M. and Stolper E. (1984) Crystallization experiments on a range of Ca–Al-rich inclusion compositions (abstract). *Lunar Planet. Sci.* **XV**, 631–632.

Petaev M. I. and Wood J. A. (2005) Meteoritic constraints on temperatures, pressures, cooling rates, chemical compositions, and modes of condensation in the solar nebula. In *Chondrites and the Protoplanetary Disk*, vol. 341 (eds. A. N. Krot, E. R. D. Scott, and B. Reipurth). Astronomical Society of the Pacific Conference Series, pp. 373–407

Richter F. M., Davis A. M., Ebel D. S. and Hashimoto A. (2002) Elemental and isotopic fractionation of type B calcium-, aluminum-rich inclusions: experiments, theoretical considerations, and constraints on their thermal evolution. *Geochim. Cosmochim. Acta* **66**, 521–540.

Stolper E. (1982) Crystallization sequences of Ca–Al-rich inclusions from Allende: an experimental study. *Geochim. Cosmochim. Acta* **46**, 2159–2180.

Stolper E. and Paque J. M. (1986) Crystallization sequences of Ca–Al-rich inclusions from Allende: the effects of cooling rate and maximum temperature. *Geochim. Cosmochim. Acta* **50**, 1785–1806.

Tissandier L., Libourel G. and Robert F. (2002) Gas–melt interactions and their bearings on chondrule formation. *Meteorit. Planet. Sci.* **37**, 1377–1389.

Wark D. A. (1987) Plagioclase-rich inclusions in carbonaceous chondrite meteorites: liquid condensates? *Geochim. Cosmochim. Acta* **51**, 221–242.

Yoneda S. and Grossman L. (1995) Condensation of CaO–MgO–Al_2O_3–SiO_2 liquids from cosmic gases. *Geochim. Cosmochim. Acta* **59**, 3413–3444.

Associate editor: Sara S. Russell